

Technical Report Documentation Page

1. Report No. FHWA/TX-11/0-6005-2		2. Government Accession No.		3. Recipient's Catalog No.	
4. Title and Subtitle Developing a Testing Device for Total Pavements Acceptance				5. Report Date February 2011; Revised June 2011, Published July 2012	
				6. Performing Organization Code	
7. Author(s) Kenneth H. Stokoe, II, Loukas F. Kallivokas, Boo H. Nam, Claire K. Carpenter, Jung-Su Lee, Adam D. Bryant, Damon A. Weeks, Richard Hayes (CTR); Thomas Scullion and Wenting Liu (TTI)				8. Performing Organization Report No. 0-6005-2	
9. Performing Organization Name and Address Center for Transportation Research The University of Texas at Austin 1616 Guadalupe St, Suite 4.202 Austin, TX 78701 Texas Transportation Institute Texas A&M University System 3135 TAMU College Station, Texas 77843-3135				10. Work Unit No. (TRAIS)	
				11. Contract or Grant No. 0-6005	
12. Sponsoring Agency Name and Address Texas Department of Transportation Research and Technology Implementation Office P.O. Box 5080 Austin, TX 78763-5080				13. Type of Report and Period Covered Technical Report 9/1/2009-8/31/2010	
				14. Sponsoring Agency Code	
15. Supplementary Notes Project performed in cooperation with the Texas Department of Transportation and the Federal Highway Administration.					
16. Abstract During the second year of Project 0-6005, significant progress was made towards building the Total Pavement Acceptance Device (TPAD). The TPAD will be a multi-function device that will be used to profile continuously along pavements at speeds in the range of 5 to 10 mph. The test functions will include those associated with Rolling Dynamics Deflectometer (RDD), ground penetrating radar (GPR), DMI and high-precision differential GPS, and surface temperature measurements, as well as digital video imaging of the pavement and right-of-way conditions. The specifications, bid documents, bid acceptances, and purchase of the TPAD mobile platform and the TPAD transportation equipment (tractor and trailer) were completed by the CTR team. Construction of the TPAD is well underway and the acceptance testing will be done in early Year 3. Progress was also made in developing (1) improved rolling sensors and associated data analysis methods commensurate with the target testing speeds and (2) a second-generation integrated data acquisition and display system which records all test functions on the same time and distance baselines.					
17. Key Words Continuous Deflection Profiling, Testing Speed, GPR and GPS Measurements, Video Imaging, Single Moving Platform			18. Distribution Statement No restrictions. This document is available to the public through the National Technical Information Service, Springfield, Virginia 22161; www.ntis.gov.		
19. Security Classif. (of report) Unclassified		20. Security Classif. (of this page) Unclassified		21. No. of pages 88	
22. Price					



Developing a Testing Device for Total Pavements Acceptance

CTR

Kenneth H. Stokoe, II
Loukas F. Kallivokas
Boo H. Nam
Claire K. Carpenter
Jung-Su Lee
Adam D. Bryant
Damon A. Weeks
Richard Hayes

TTI

Thomas Scullion
Wenting Liu

CTR Technical Report:	0-6005-2
Report Date:	February 2011; Revised June 2011
Project:	0-6005
Project Title:	Developing a Testing Device for Total Pavements Acceptance
Sponsoring Agency:	Texas Department of Transportation
Performing Agency:	Center for Transportation Research at The University of Texas at Austin

Project performed in cooperation with the Texas Department of Transportation and the Federal Highway Administration.

Center for Transportation Research
The University of Texas at Austin
1616 Guadalupe St, Suite 4.202
Austin, TX 78701

www.utexas.edu/research/ctr

Copyright (c) 2011
Center for Transportation Research
The University of Texas at Austin

All rights reserved
Printed in the United States of America

Disclaimers

Author's Disclaimer: The contents of this report reflect the views of the authors, who are responsible for the facts and the accuracy of the data presented herein. The contents do not necessarily reflect the official view or policies of the Federal Highway Administration or the Texas Department of Transportation (TxDOT). This report does not constitute a standard, specification, or regulation.

Patent Disclaimer: There was no invention or discovery conceived or first actually reduced to practice in the course of or under this contract, including any art, method, process, machine manufacture, design or composition of matter, or any new useful improvement thereof, or any variety of plant, which is or may be patentable under the patent laws of the United States of America or any foreign country.

Engineering Disclaimer

NOT INTENDED FOR CONSTRUCTION, BIDDING, OR PERMIT PURPOSES.

Project Engineer: Kenneth H. Stokoe, II
Professional Engineer License State and Number: Texas No. 49095
P. E. Designation: Research Supervisor

Acknowledgments

The research team wishes to express its sincere gratitude to TxDOT for supporting this research project. The interaction and support from the Research Monitoring Committee—Mr. Joe Leidy, Mr. Ed Oshinski, Dr. Dar Hao Chen, and Dr. German Claros—has been very important to the progress of the project. The UT Staff—Mr. Cecil Hoffpauir, Mr. Curtis Mullins, and Dr. Farn-Yuh Menq—helped significantly in the field tests with the UT RDD used in developing improved rolling sensors and an improved data analysis software, as well as evaluating new data collection hardware. We owe much to Industrial Vehicles Incorporated (ivi) for developing the prototype ivi RDD that was used in Year 1. The generosity of Mr. Jay Bird, Mr. Elmo Christensen, and Mr. Mike Grady of ivi in sharing their ideas and the prototype vehicle with us, at no cost to the project, also in Year 2 is greatly appreciated. Finally, we are grateful to Mr. Don Ramsey and the personnel of the TxDOT Flight Services Facility for their kindness in allowing us to develop and use a pavement testbed at their facility.

Table of Contents

Chapter 1. Introduction.....	1
1.1 Project Objectives and Overview	1
1.2 Outline of Progress during Year 2	1
Chapter 2. Specifications, Construction, and Purchase of TPAD Mobile Platform and Transportation Equipment.....	3
2.1 Introduction and Overview	3
2.2 Construction of the Mobile TPAD Platform.....	6
2.3 Purchase of the Tractor and Trailer	6
Chapter 3. Improvements to the RDD Rolling Sensors.....	9
3.1 Introduction.....	9
3.2 Description of the RDD Portion of the TPAD.....	9
3.3 History of Previous Rolling Sensors.....	10
3.3.1 First-Generation Rolling Sensor	10
3.3.2 Second-Generation Rolling Sensor.....	11
3.4 Speed-Improved Rolling Sensor Design by the CEM.....	12
3.5 Parameters Affecting the Performance of Rolling Sensors	19
3.5.1 Stiffness of Urethane Wheel Tread: Urethane Hardness and Thickness	19
3.5.2 Sensor Hold-Down Force.....	22
3.6 Rolling Noise Measurement	24
3.6.1 Rolling Noise Characteristics and Signal-to-Noise Ratios	24
3.6.2 Measurement of Continuous Noise-Level Deflection Profiles	27
3.7 Deflection Measurements	29
Chapter 4. Improvements to the RDD Data Analysis Procedure.....	35
4.1 Introduction.....	35
4.2 Original RDD Data Analysis	35
4.2.1 Overview of the Original Data Processing	35
4.2.2 Limitations of the Original RDD Data Processing	38
4.3 Improved Data Analysis Procedure	39
4.3.1 Distance-Based Analysis	39
4.3.2 Distance-Based Analysis with Moving Average	41
Chapter 5. RDD Data Acquisition Software Development	47
5.1 Introduction.....	47
5.2 Software Development	47
5.3 Hardware Development	49
5.4 Field Testing of New TPAD Data Acquisition System with the Original TPAD	52
Chapter 6. Summary of Year 2 Activities.....	55
References.....	57
Appendix A: Specifications for RDD Vehicle Portion of the TPAD	59
Appendix B: Design and Fabrication of Improved Rolling Sensor.....	71

List of Figures

Figure 2.1: Photographs of the TPAD Mobile Platform Under Construction at ivi in Tulsa, OK.....	5
Figure 2.2: TPAD Transportation Equipment that was Ordered in July 2010: (a) Tractor and (b) Trailer	7
Figure 3.1: General RDD Arrangement with Rolling Sensor Array: (a) Original Rolling Dynamic Deflectometer, and (b) a Typical Rolling Sensor Configuration for RDD Testing.....	10
Figure 3.2: Photographs of RDD Rolling Sensors: (a) First-Generation Rolling Sensor and (b) Second-Generation Rolling Sensor	11
Figure 3.3: Depiction of Sensor Wheels of Different Diameter Rolling over Random Surface Roughness (from Bay and Stokoe 1998).....	14
Figure 3.4: Effect of Sensor Wheel Width; Average Vertical Displacements from a 6-in. Diameter Rigid Wheel over the Synthesized Pavement Surface (Bay and Stokoe 1998)	15
Figure 3.5: Progress of the New RDD Sensor Construction: (a) Carts and Interchangeable Wheel Sets and (b) Bearing Set with Different Axles	16
Figure 3.6: Proposed Hold-Down Mechanisms of the Rolling Sensor: (a) Single-Wheel Concept, (b) Current ivi Sensor, and (c) Force-Actuator Concept	18
Figure 3.7: Information of Urethane Hardness and Its Physical Properties (from PSI Urethane Inc. 2009)	20
Figure 3.8: Noise Measurements (No RDD Dynamic Loading) Using a Two-Wheel Rolling Sensor with Wheel Tread Urethanes of 70A and 80A; Linear Spectra of a 5-second Measurement Window at Different Speeds of 1, 3, and 5 mph	21
Figure 3.9: Dynamic Response of a Rolling Sensor with Different Urethane-Tread Thicknesses: (a) 0.25-in. Thick Urethane, (b) 0.5-in. Thick Urethane, and (c) 0.75-in. Thick Urethane	23
Figure 3.10: Field Sensor Calibration of the Second-Generation Sensor with a 50 A Urethane Tread: (a) Calibration Curves with Hold-Down Forces of 0, 2, and 4 psi and (b) Calibration Curves of the Sensor with 50 A and 50 D.....	24
Figure 3.11: Rolling Noise Characteristics and Signal-to-Noise Ratio (SNR): (a) Rolling Noise Definition, (b) SNR Calculation, and (c) Generalized Relationship between Rolling Noise, Test Speed, and Pavement Surface Roughness (from Lee 2006).....	26
Figure 3.12: Noise-Level Deflection Profiles at 1 mph Using the Second-Generation Old and New Rolling Sensors Collected along Path E at the TxDOT FSF	28
Figure 3.13: Noise-Level Deflection Profiles at 3 mph Using the Second-Generation Old and New Rolling Sensors Collected along Path E at the TxDOT FSF	28
Figure 3.14: Noise-Level Deflection Profiles at 5 mph Using the Second-Generation Old and New Rolling Sensors Collected along Path E at the TxDOT FSF	29

Figure 3.15: Continuous Deflection Profile at 1 mph Using the New Rolling Sensor along Path E at the TxDOT FSF	30
Figure 3.16: Continuous Deflection Profiles at 1 and 3 mph Using the New Rolling Sensor along Path E at the TxDOT FSF	31
Figure 3.17: Continuous Deflection Profiles at 1 and 5 mph Using the New Rolling Sensor along Path E at the TxDOT FSF	31
Figure 3.18: Continuous Deflection Profiles at 1 mph Using the Old and New Rolling Sensors Collected along Path E at the TxDOT FSF	32
Figure 3.19: Continuous Deflection Profiles at 3 mph Using the Old and New Rolling Sensors Collected along Path E at the TxDOT FSF	33
Figure 3.20: Continuous Deflection Profiles at 5 mph Using the Old and New Rolling Sensors Collected along Path E at the TxDOT FSF	33
Figure 4.1: Flow Chart of Original RDD Data Processing to Calculate Dynamic Displacement versus Distance from the RDD Sensor Outputs.....	38
Figure 4.2: Deflection Profiles Constructed by Time- and Distance-Based Methods; Data Set Collected along a JCP Using the First-Generation Rolling Sensor (Sensor #1) at 1 mph: (a) Time-Based Deflection Profile with Time Interval of 1 sec and (b) Distance-Based Deflection Profile with Distance Interval of 1.5 ft	40
Figure 4.3: RDD Distance-Based Deflection Profiles with Different Spatial Resolutions of 1, 1.5, and 2 ft; Data Set Collected along a JCP Using the First-Generation Rolling Sensor (Sensor #1) at 1 mph	41
Figure 4.4: Expanded View of Moving Average Distance-Based Profile at a Joint; Distance Interval of 2 ft and Delta (Δ) of 1 ft.....	42
Figure 4.5: RDD Deflection Profiles at a Speed of 1 mph: (a) Moving-Average Deflection Profile (Distance Interval of 1.5 ft and Delta of 0.5 ft) along Path E and (b) Expanded View of Moving-Average and Time-Based Deflection Profiles at Joint A.....	44
Figure 4.6: RDD Deflection Profiles at a Speed of 3 mph: (a) Moving-Average Deflection Profile (Distance Interval of 3 ft and Delta of 1 ft) along Path E and (b) Expanded View of Moving-Average and Time-Based Deflection Profiles at Joint B.....	45
Figure 5.1: TPAD Data Channel Setup and Configuration Dialog Box.....	48
Figure 5.2: TPAD Data Acquisition Control Screen	48
Figure 5.3: Real Time TPAD Data Acquisition Screen.....	49
Figure 5.4: TPAD Data Acquisition Hardware System Setup Diagram.....	50
Figure 5.5: TPAD Data Acquisition Instrument Box	50
Figure 5.6: TPAD Data Acquisition Instrument Box (When Closed).....	51
Figure 5.7: New GPR Control Box for the TPAD Data Acquisition System.....	51
Figure 5.8: Mounting the GPS, GPR and Digital Video System on the Original TPAD Unit	52
Figure 5.9: Loading Roller and Rolling Sensors Arrangement Used in Testing	53
Figure 5.10: Test location and test path at TxDOT FSF.....	53

Figure 5.11: Geophone velocity data for each run.....	54
Display of Raw data during data aquisition.....	54
Figure A1: Location of Loading Rollers.....	64
Figure A2: Front and Side Views	65
Figure A3: Bottom Views.....	66
Figure A4: Side View Showing Sensor Layout and Space Claim Detail.....	67
Figure A5: Detailed Views	68
Figure A6: Space Requirement for TTI Data Acquisition System in Cab of New RDD	69
Figure B1: New Rolling Sensor Designed by the CEM.....	71
Figure B2: Mechanical Drawings of the Sensor Wheel and New Bearing Set	72
Figure B3: Photographs of the New Rolling Sensor of the TPAD.....	73

Chapter 1. Introduction

1.1 Project Objectives and Overview

The primary objective of Project 0-6005 is to develop the Total Pavement Acceptance Device (TPAD), which is a new nondestructive testing device that will be used to continuously assess pavement structural conditions. The TPAD will be a multi-function device that includes the capacities of the Rolling Dynamic Deflectometer (RDD), Ground Penetrating Radar (GPR), Distance Measurement Instrument (DMI), and high-precision differential GPS measurements. In addition, pavement surface temperature measurements and digital video imaging of the pavement will be included.

This 3-year project began in September 2008. The second-year efforts are discussed in this report. It is a joint effort between the Center for Transportation Research (CTR) at the University of Texas (UT) and the Texas Transportation Institute (TTI) at Texas A&M University. Researchers at CTR, working with researchers at the Center for Electromechanics (CEM) at UT, are responsible for developing all aspects dealing with the RDD portion of the TPAD. This work includes developing (1) the specifications, construction, and purchase of TPAD mobile platform and transportation equipment, (2) improvements of RDD rolling sensors, and (3) improvements of RDD data analysis procedure.

1.2 Outline of Progress during Year 2

The TPAD is being developed in several phases, some in parallel and some sequentially. Critical starting points are the following: (1) make appropriate specifications for the moving platform on which to house the dynamic loading and deflection measurement systems associated with the RDD portion of the TPAD, (2) with this platform, evaluate the performance of the TPAD mobile platform, (3) select appropriate transportation equipment for the TPAD mobile platform, (4) develop a speed-improved rolling sensor for the RDD function, and (5) develop the data-analysis software necessary to permit continuous moving measurements to be performed at speeds in the range of 5 to 10 mph. Significant progress has been made in these areas as discussed in Chapters 2 through 4. The moving platform for the TPAD is a modified version of a unique truck-mounted device manufactured by Industrial Vehicles Incorporated (ivi) of Tulsa, Oklahoma. Specifications and progress of construction and purchase of TPAD mobile platform and transportation equipment are described in Chapter 2. Efforts to improve the RDD rolling sensors to achieve the target speed of 5 mph or more are presented in Chapter 3. Speed-improved rolling sensors, designed by CEM personnel, have been fabricated. Additional studies were conducted to find the optimum conditions of parameters affecting the sensor performance (i.e., hardness, thickness, and width of the cart-wheel treads made of urethane and the sensor hold-down system). A series of field tests were performed at the TxDOT Flight Service Facility (FSF) at the Austin Bergstrom International Airport to evaluate their performance associated with rolling noise at higher test speeds. Chapter 4 discusses enhancements to the RDD data analysis procedure to improve spatial resolution in the RDD deflection data without sacrificing performance of a band-pass digital filter. Chapter 5 discusses the development of the RDD data acquisition software. To conclude the report, Chapter 6 summarizes the path followed in Year 2.

Chapter 2. Specifications, Construction, and Purchase of TPAD Mobile Platform and Transportation Equipment

2.1 Introduction and Overview

Specifications, construction, and purchase of the TPAD mobile platform and transportation equipment are discussed in this chapter. The specifications of the TPAD mobile platform can be divided into two portions: (1) the RDD vehicle portion of the TPAD and (2) the RDD dynamic loading unit portion of the TPAD. Photographs of the TPAD mobile platform are shown in Figure 2.1. A summary of the specifications of the mobile platform is presented herein, with more details presented in Appendix A. In the vehicle portion of the TPAD, the following eight items are considered:

- (1) Vehicle: shall be four-wheel drive hydrostatically driven with planetary type drive axles with locking differentials. Vehicle weight shall not exceed 20,000 lbs.
- (2) Tires: vehicle shall have R4 14.9x224 8-ply Turf tread tires or equivalent.
- (3) Cab: two-man cab with a minimum 142 cubic feet, which is the minimum space to house the two-man crew and associated data acquisition systems.
- (4) Instrumentation: unit shall be equipped with specified gauges, indicators, and alarms.
- (5) Engine: shall be a diesel engine and have a minimum of 115 horsepower at 2,500 rpm continuous rating with minimum 291-ft-lbs torque at 1,400 rpm, which represents the minimum power required to perform the RDD functions and support the other TPAD functions.
- (6) Fuel Tank Capacity: minimum 40 gallons, which is an industry standard.
- (7) Hydraulic System: vehicle hydraulic system provides minimum 3,000 psi pressure to the vehicle drive system, which is an industry standard.
- (8) Safety Plaques or Decals: product safety plaques and decals shall be affixed to the vehicle.

In the dynamic loading portion of the TPAD, the following six items are considered:

- (1) Dynamic Loading Unit: provides dynamic sinusoidal force covering a range of 2,000 to 20,000 lbs peak to peak.
- (2) Dynamic Force Measurement: install accelerometers to monitor the dynamic force level.
- (3) Static Hold-Down System: applies a static force (in the range of 2,000 to 12,000 lbs) to the two loading rollers.
- (4) Static Hold-Down System Operations: the static hold-down system shall be operated from the cab of the vehicle.
- (5) Loading Rollers: delivers static and dynamic forces to the pavement.

- (6) Location and Clear Space Required for Sensing Rollers: the locations of the rolling sensors, areas of required space claim, and locations for potential mounting points are illustrated in Appendix A.



(a) Side View of the TPAD Platform



(b) Rear View of the TPAD Platform

Figure 2.1: Photographs of the TPAD Mobile Platform Under Construction at ivi in Tulsa, OK

2.2 Construction of the Mobile TPAD Platform

After the specifications for the Mobile Platform were reviewed and approved, Dr. Kenneth Stokoe initiated the process of obtaining the sole source purchase authority from the Purchasing Department at The University of Texas at Austin to purchase the mobile platform from Industrial Vehicles International (ivi) in Tulsa, Oklahoma. After the sole source authority was approved, a purchase order was sent to ivi on June 7, 2010 to purchase the Mobile TPAD Platform. CTR personnel were in contact with ivi throughout the initial construction process.

2.3 Purchase of the Tractor and Trailer

In November 2009, UT personnel initiated the process to obtain specifications for the tractor (truck) and trailer to haul and support the Mobile TPAD Platform. The objective was to purchase a tractor that was capable of handling the trailer and load, in all adverse conditions, and had the capacity to haul and store the support equipment for the TPAD. The Mobile TPAD Platform has to be hauled to the location of the pavement and cannot be driven at speeds more than about 15 to 20 mph. The mobile platform has spare parts and other support equipment used to repair simple damage or breakdowns that may occur during normal operations on a pavement. The objectives were to purchase a trailer that had minimum load angle so the TPAD could easily drive onto the trailer and had the capacity to safely haul the Mobile Platform and supporting equipment.

On June 7, 2010, the purchase order for the Mobile Platform was sent to ivi, and on June 8, 2010, the process to obtain authority to purchase the tractor and trailer was initiated. In the first week of July, 2010, The University of Texas at Austin sent the purchase order for the tractor and trailer to Freightliner of Austin, TX. The tractor and trailer equipment that was ordered are shown in Figure 2.2.



(a)



(b)

*Figure 2.2: TPAD Transportation Equipment that was Ordered in July 2010:
(a) Tractor and (b) Trailer*

Chapter 3. Improvements to the RDD Rolling Sensors

3.1 Introduction

As discussed in Chapter 1, development and improvement of the RDD rolling sensors for the TPAD have been made. This work was performed as part of Task 4 of Project 0-6005. The studies involved the original UT RDD that was used to perform measurements at stationary (field sensor calibration) and rolling (noise and deflection measurements) modes at the TxDOT FSF. The speed-improved rolling sensors were designed by the Center for Electromechanics (CEM). They utilize larger-diameter wheels (9.5 in. or 12.5 in.), softer and thicker urethane wheel treads, new bearing sets, and a new sensor hold-down mechanism. Additional studies were performed in Year 2 to find the optimum parameters affecting the performance of the rolling sensors. These parameters are (1) hardness and thickness of the urethane wheel tread, (2) width of the sensor wheel, and (3) the sensor hold-down force. To evaluate these parameters, deflection and noise measurements with the original UT RDD were performed along a 700-ft section of jointed concrete pavement at the TxDOT FSF. In addition, field sensor calibrations were performed in a mid-slab area in the stationary mode.

3.2 Description of the RDD Portion of the TPAD

The RDD portion of the TPAD is mounted on a moving platform and is composed of three major systems that are: (1) a dynamic loading and force measurement system, (2) a rolling sensor system, and (3) a distance measurement system. A schematic diagram of the RDD, using the original RDD and the arrangement of the rolling sensors are shown in Figure 3.1. Each rolling sensor is composed of three rolling wheels and a 2-Hz geophone at the geometric center of the three wheels. With the first-generation rolling sensors, the original RDD was used to profile along the pavement at approximately 1 mph. The improved RDD-portion of the TPAD is being designed to profile at 5 mph or more.

During RDD testing, both static and dynamic forces are applied to the pavement through two loading rollers. The RDD loading system in the TPAD will be able to generate static forces of 2 to 12 kips and dynamic sinusoidal forces with a peak-to-peak amplitude of 2 to 20 kips over the frequency range of about 20 to 50 Hz. In typical highway rehabilitation projects with the original RDD (Bay and Stokoe, 1998 and Chen et al., 2007), a static hold-down force in the range of 8 to 10 kips and a peak-to-peak dynamic force in the range of 8 to 10 kips at an operating frequency of 30 Hz have been used. These forces and loading frequencies are well within the operating range of the TPAD. The combined static and dynamic forces can be continuously recorded by multiple accelerometers on the loading platform. The two or more sensors under the RDD measure the pavement movements (dynamic deflections) under the sinusoidal loading. A distance measurement system on the drive shaft of the moving platform is used to measure the distance traveled along the pavement. The output signals from accelerometers (loads), rolling sensors, and distance measurement are individually recorded and synthesized to produce the continuous deflection profile.

In the RDD data processing, a digital notch-pass filter is used to remove noise from the recorded signals. Since the RDD operating frequency is known during testing (typically 30 Hz), the filtered output signals have the same frequency as the dynamic loading (input). The filtered signals are averaged over a distance of approximately 2 ft for a 1-mph speed and converted to dynamic deflections. The RDD loading can vary due to rough pavement surface, varying

pavement support and, acceleration and deceleration of the moving platform while traveling. To minimize deflection differences due to load variations, the deflections are continuously normalized by the applied dynamic load and presented as deflections under a 10-kip load.

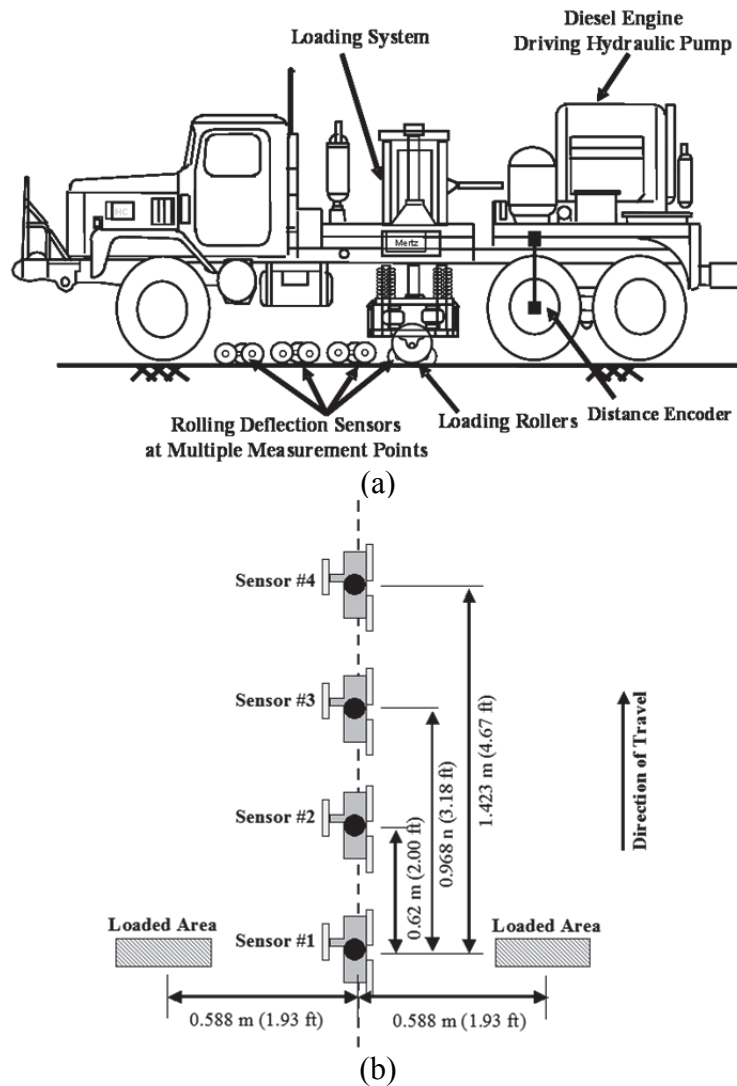


Figure 3.1: General RDD Arrangement with Rolling Sensor Array: (a) Original Rolling Dynamic Deflectometer, and (b) a Typical Rolling Sensor Configuration for RDD Testing.

3.3 History of Previous Rolling Sensors

3.3.1 First-Generation Rolling Sensor

The first-generation rolling sensors were developed at UT. These sensors are freestanding systems, with each system composed of three rolling wheels and a 2-Hz geophone in the geometric middle of the three wheels. A photograph of a first-generation rolling sensor is shown in Figure 3.2a. Each rolling wheel is 6 in. in diameter and 1 in. in width. The wheels have a 0.25-in. thick coating of soft (60A durometer) urethane cast on the rims.

With the first-generation sensors, the testing speed of the RDD is less than or equal to 1 mph. This speed limitation is due to sensor decoupling and rolling noise. The first-generation sensor wheels have a tendency to decouple from the ground while rolling at speeds higher than 1 mph because of no additional hold-down mechanism except its self weight. If the induced acceleration of the sensor exceeds -1 g, the force between the sensor and the pavement is zero. In other words, the sensor wheel likely loses contact with the pavement, resulting in inappropriate measurements of the pavement deflections induced by the RDD dynamic loading. Although the sensor is in contact with the pavement, increasing the speed results in dramatically increasing the rolling noise over the complete frequency range. Doubling the rolling velocity almost doubles the amplitude of the rolling noise (Bay and Stokoe, 1998).

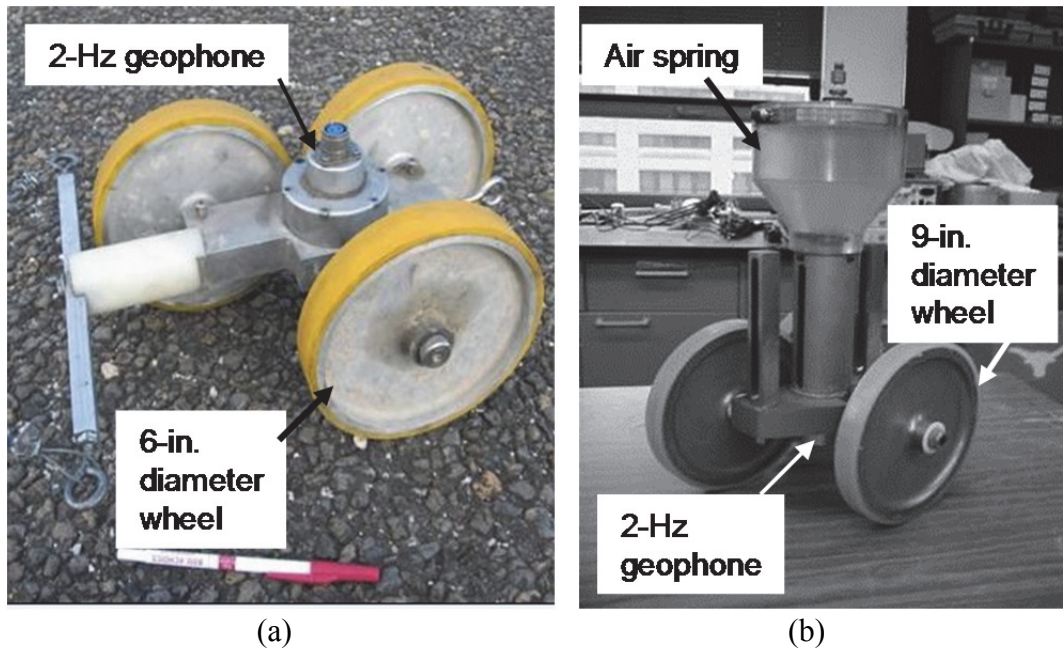


Figure 3.2: Photographs of RDD Rolling Sensors: (a) First-Generation Rolling Sensor and (b) Second-Generation Rolling Sensor

3.3.2 Second-Generation Rolling Sensor

Second-generation rolling sensors were developed to improve the test speed of the RDD up to 2 or 3 mph (Lee, 2006). The second-generation sensors use larger diameter wheels and an air spring as a hold-down force. The photograph of the second-generation rolling sensor is shown in Figure 3.2b. The larger diameter wheels are less sensitive to rough pavement surfaces and the hold-down force can keep the rolling sensor in contact with the pavements at higher testing speeds. This hold-down force is applied to the top of each rolling sensor through an inflatable polyurethane air-spring (typically pressurized to 5 psi). Generally, only two rolling sensors are used at the locations of Sensors #1 and #3, as shown in Figure 3.1b. Second-generation Sensor #1 has 9-in. diameter wheels and second-generation Sensor #2 has 12-in. diameter wheels. The smaller wheels of Sensor #1 are the result of limited vertical space that exists between the two loading rollers.

However, several field tests have revealed a number of technical limitations of the second-generation rolling sensors. The testing speed of 3 mph might, at times, induce some

instability in the sensors from a mechanical view point. The second-generation sensors have no additional system to align the sensor other than the air spring on top of the sensor (Note: These limitations are being addressed in the TPAD rolling sensors, although the final solution has not yet been reached). Sensor #1 in the middle of the loading platform is space limited in the horizontal and vertical directions. Thus, horizontal movements of Sensor #1 cannot be allowed so that Sensor #1 does not contact the loading platform, resulting in erroneous deflections. This problem has been observed several times on rough surfaces, such as around potholes or faulting. In addition, the second-generation sensor measures slightly lower deflections at joints and cracks than the first-generation sensor. At joints, a deflection measured using the three-wheel contact points represents an average deflection rather than a point deflection. For jointed concrete pavements (JCPs), as the RDD passes transverse joints, all three wheels of the sensor cannot be positioned on the same side of the loaded slab at the point of maximum motion. Generally, larger diameter wheels will involve a larger portion away from the joint, resulting in measuring lower joint deflections. This point of averaging deflections will always exist with this type of rolling sensors but improved data capture and processing are lessening the problem.

3.4 Speed-Improved Rolling Sensor Design by the CEM

Based on the modeling and analysis completed in Year 1 of this project, CEM recommended a number of areas where noticeable gains in performance could likely be achieved. These included:

- Reducing rolling noise sources and improving tracking with better wheels and bearings.
- Utilizing wider, more compliant sensor wheels to reduce impact of disparities.
- Utilizing larger diameter wheels to reduce road noise.
- Implementing an active actuator to provide a more constant hold down force.
- Modifications to the loading-roller system to reduce resonant and transmitted vibrations.
- Integrating a sensor into the loading rollers.
- Replacing or supplementing geophones with an inertial measurement system, stabilized with an active suspension system.
- Using an external analog integrator of the geophone signal.

Based on previous analysis and observations that indicated that a high chance of success could be proven through near-term testing, CEM and CTR decided to focus on the first three recommendations noted above for immediate pursuit. The background and efforts associated with implementing these options are presented in the following pages. A concept for the fourth recommendation, which incorporated an active actuator, was developed and is also presented in this report. However, it was not implemented, due to time and budget constraints. The fifth recommendation was deemed primarily valid for the original UT RDD, as opposed to the ivi system and was not pursued. The remaining recommendations all offer opportunity for improvement and could be pursued in the future if time and funding are available.

To establish a baseline and evaluate the type of data collected, acceleration data were collected with the current three-wheel sensor package, shown in Figure 3.2a, mounted to the original UT RDD vehicle, with the sensor package isolated from the vehicle and its external loading frame. From observations and interpretation of the collected data, the researchers decided to redesign the rolling sensor contact wheels and made a number of material and component changes. The wheels were redesigned to have a larger contact area and to use a softer urethane wheel tread. Specific improvements made to the bearing arrangements and wheel mounting included:

- Relocating the wheels to accommodate a wider footprint.
- Incorporating rolling element bearings vs. bushings to reduce noise and improve tracking.
- Using wider (4 in. and 2 in. versus 1 in. and 2 in.) wheels to increase tire contact patch.
- Making the tread area on each side of the cart equal for better tracking.
- Reducing tire modulus to reduce impact of small disparities in the road surface while maintaining the same overall wheel stiffness with wider tire patch.
- Providing larger diameter wheels (12 in. vs. 9 in.) as an option for future testing.

The decision to implement these specific changes was driven by CEM's analysis and also by the previous work of Bay and Stokoe (1998), which described the sensor wheel rolling over a road surface with random roughness as contacting only the high points. This work assumed an idealized rigid wheel interacting with a 2-D rough surface, as shown in Figure 3.3. The result of this interaction is that the axles of different diameter wheels would travel along different arcs. This theory predicts that wheels with a larger diameter will have lower rolling noise. However, in practice, there is a practical limit as to how large a wheel can be implemented on the TPAD.

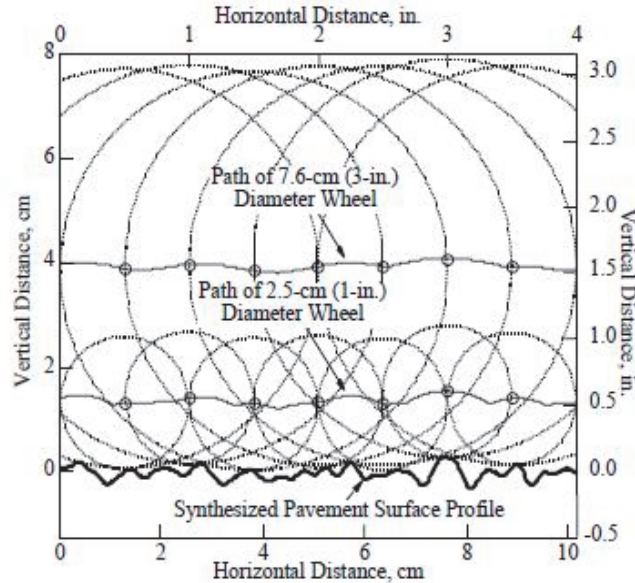


Figure 3.3: Depiction of Sensor Wheels of Different Diameter Rolling over Random Surface Roughness (from Bay and Stokoe 1998)

Bay and Stoke (1998) then projected the 2-D terrain into 3-D space to determine the effect of wheel width. Similarly, they found that initially axle displacements steadily reduced for increasing wheel widths up to approximately one inch as shown in Figure 3.4. Finally, they investigated wheel compliance on rolling noise. In the analysis, they stated that the rolling noise might be reduced by using a compliant tire material but were concerned about the potential resonance interactions with measurements that could be created by the compliant tire and wheel mass. Some laboratory testing was mentioned but no conclusive results were presented. The CTR and CEM team during this reporting period proposed an approach to exploit higher tire compliance without the potential liability of detrimental resonance interactions.

In work under Phase I of this project, transfer functions that described the measurement system dynamics were developed. Based on the transfer function analysis, it was found that the geophone cart deflections could be kept proportional to the ground deflections if the pavement excitation frequency was greater than the carriage natural frequency and less than the wheel natural frequency. Based on the current geophone-cart design, the carriage natural frequency is on order of a few hertz, while the wheel natural frequency is of the order of 100-200 Hz. Currently, the RDD loading system utilizes 30-Hz excitation of the vibration system load roller. To further reduce the rolling noise while maintaining a high wheel resonance, it was hypothesized that a softer tire material could be combined with a wider wheel. This approach would allow local asperities to deform the soft tire surface while at the same time the larger surface area provides high average stiffness. During this reporting period, engineers from CTR and CEM met with PSI Urethane of Austin, Texas, to discuss softer durometer tire materials. Representatives from PSI demonstrated various urethane samples. The researchers decided to use tire materials with a durometer of 80A and 70A in place of the currently used 60D. To maintain the tire stiffness with softer durometer urethane treads, wider wheels were developed.

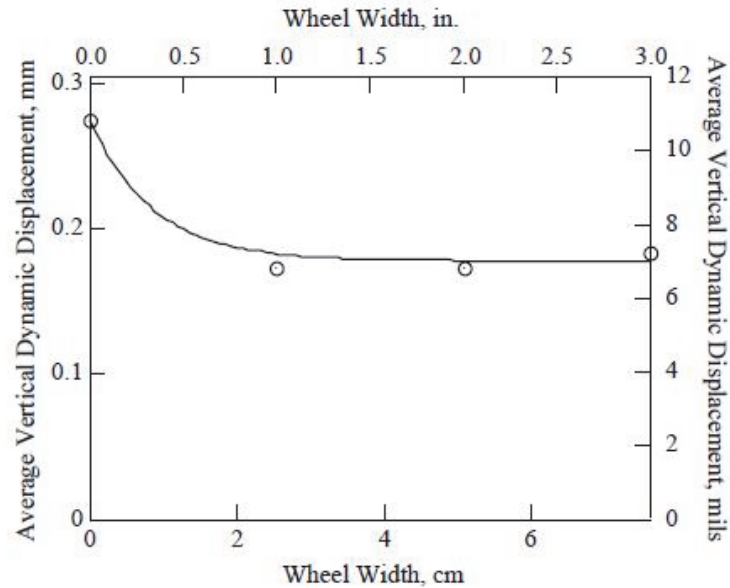


Figure 3.4: Effect of Sensor Wheel Width; Average Vertical Displacements from a 6-in. Diameter Rigid Wheel over the Synthesized Pavement Surface (Bay and Stokoe 1998)

Based on the results of this analysis, a full complement of wheels of varying widths and diameters and carts was fabricated during this second year. All of the wheels were redesigned to incorporate a new rolling element bearing design specified by CEM to reduce rolling resistance, improve tracking, and improve signal fidelity when compared to the bushings previously incorporated on the sensor carts. The wheels and carts are all interchangeable to allow a wide variety of configuration changes which will allow the team to develop the best combination as the project continues. Manufacturing drawings and photographs for all fabricated parts and the sensor assembly are presented in Appendix B. The hardware, fabricated and purchased, is shown in Figure 3.5a. This hardware includes:

- four sensor cart bodies,
- four complete bearing sets (one set covers 3 wheels),
- four 9-in. diameter wheels that are 4-in. wide,
- eight 9-in. diameter wheels that are 2-in. wide,
- eight 9-in. diameter wheels that are 1-in. wide,
- two 12-in. diameter wheels that are 4-in. wide,
- four 12-in. diameter wheels that are 2-in. wide,
- four 12-in. diameter wheels that are 1-in. wide, and
- bearings, seals, locknuts, and retaining rings.



(a)



(b)

Figure 3.5: Progress of the New RDD Sensor Construction: (a) Carts and Interchangeable Wheel Sets and (b) Bearing Set with Different Axles

Following the fabrication and assembly of the redesigned sensor wheels and sensor cart, work was initiated on enhancement of the three-wheel sensor hold-down mechanism to improve stability and reduce required under-vehicle clearance. During this time period, a single, wide, contacting wheel with a trailing-arm type suspension and restraint system (see Figure 3.6a) was

also investigated. This option was ultimately rejected due to complexity and limitations that would arise in integrating it on the ivi RDD and uncertainties about performance benefits.

As a result of CEM's unsuccessful efforts to integrate the single wheel design, a new option to improve the current ivi sensor array was developed that should lead to a more tunable, higher performance system. While this design was not fully developed or fabricated due to time and budget limitations on the current project, a concept design has been developed that could be integrated into the current ivi design. Figure 3.6b shows the current ivi sensor array and Figure 3.6c shows a concept design for a sensor array that integrates an active actuator component for a hold-down mechanism. These figures indicate that an active hold-down system could be incorporated with the current ivi sensor carriage configuration, based on the size of the components and the space available.

Replacing the passive spring elements in the sensor carrier with active suspension elements appears to offer significant performance benefits on the RDD. The proposed system would include an actuator to replace the passive spring and damping elements which provide sensor hold down force in the current ivi design. This approach also attempts to leverage the work of Bay and Stokoe (1998) which suggests that the maximum speed on the RDD rolling sensor package may be improved by increasing the hold-down force. In addition, it leverages work performed in earlier parts of this effort which determined the interaction of the sensor system response with the carriage system response and indicated that it was desirable to keep carriage response frequency as low as possible (within the practical boundaries imposed by friction) so as to not interact with the sensor carriage response. By using an active element to supply the hold-down force, the sensor carriage dynamics and hold-down force may be adjusted pseudo-independently. This proposed effort also leverages CEM's expertise in active suspension. CEM has been developing active suspension systems, primarily for military vehicles, for many years. These systems typically require large, heavy, long stroke, actuators, and significant auxiliaries. More recently, however, CEM has been developing very simple "voice coil" actuators for applications where forces and stroke are reduced. This type of actuator appears to be a good fit for this application as indicated in the proposed concept.

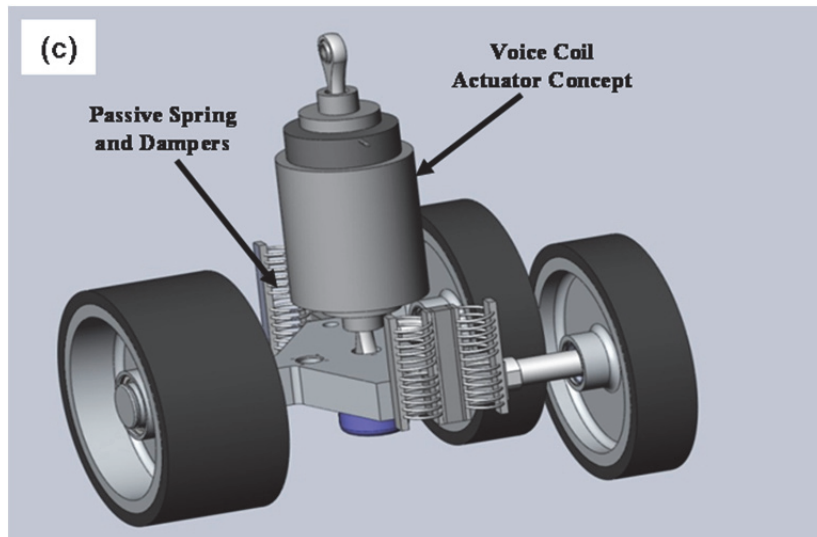
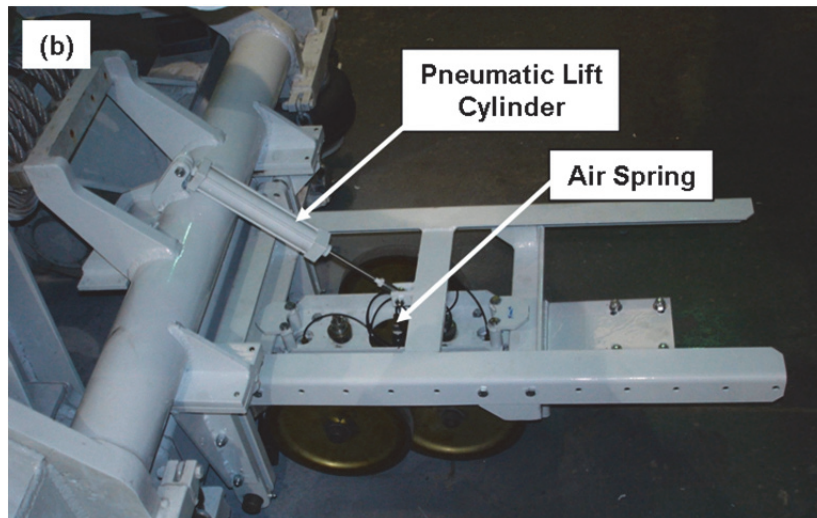
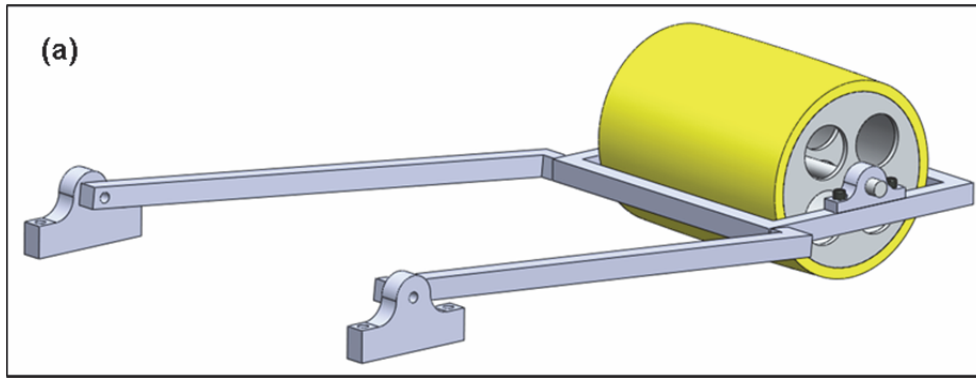


Figure 3.6: Proposed Hold-Down Mechanisms of the Rolling Sensor: (a) Single-Wheel Concept, (b) Current ivi Sensor, and (c) Force-Actuator Concept

In conclusion, CEM has developed tools to simulate and predict the performance of sensor systems mounted on the RDD. These tools have been used to examine the current system and proposed modifications in order to make recommendations for further development. Several options have been pursued and hardware has been developed by the CTR and CEM team. This equipment will be tested as soon as the TPAD moving platform is available. A range of reconfigurable sensor arrays have been fabricated and are available for additional testing. More recently a new concept for providing a controlled hold-down force, utilizing an electronically controlled actuator, on the IVI sensor cart has been developed. A proposal was submitted for funding to complete the design, fabrication, and testing of this concept, but final consideration was delayed at the end of Year 2 until the TPAD moving platform is operational.

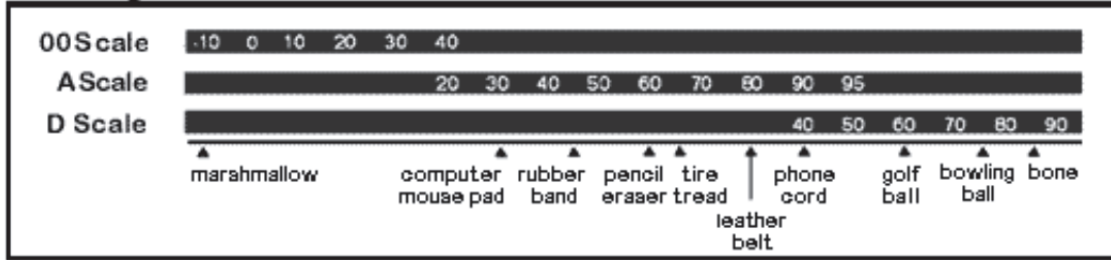
3.5 Parameters Affecting the Performance of Rolling Sensors

This section discusses additional efforts to optimize the two parameters affecting the sensor performance: (1) hardness and thickness of the urethane wheel-tread and (2) the level of the sensor hold-down force. These parameters control the dynamic response of the rolling sensor and also determine the noise level, and thus the optimized parameters allow minimizing rolling noise and maximizing signal-to-noise ratios (SNRs).

3.5.1 Stiffness of Urethane Wheel Tread: Urethane Hardness and Thickness

As a sensor wheel rolls over the pavement, a rigid wheel, such as a steel wheel, would generate high levels of high-frequency noise. On the other hand, a compliant wheel can attenuate noise and also has a decreased tendency to lose contact with the pavement. Therefore, compliant wheels need to be used in the rolling sensors, but deformation and durability of the polyurethane coating are important issues to be considered. In addition, the compliant wheels will affect the resonance of the rolling sensor. Compliant wheels can be modeled as a damped spring supporting the sensor mass, which acts as a single-degree-of-freedom (SDOF) resonator. Softer wheels will cause the resonance of the rolling sensor to move to lower frequencies range. It is desirable to have the RDD operating frequency away from the resonance frequency of the sensor.

For the wheel-tread urethane coating, the first- and second-generation sensors use polyurethane (or urethane) with a 60 durometer on the A scale and a 50 durometer on the D scale, respectively. Figure 3.7a presents a chart of the hardness of the urethane as represented by the “A” and “D” scales, which are and a scale listing common materials with similar hardnesses. Figure 3.7b also shows the physical properties of polyurethane. For the second-generation sensors, abrasion at the interface and the hold-down force of 5 psi were considered, and a 50-D urethane was selected. On the other hand, the first-generation sensors have no hold-down force, so the testing speed of 1 mph is sufficiently slow. Thus, the first-generation rolling sensor with the 60-A urethane has not had significant wear over time.



*Note: Hardness of the first-generation rolling sensors = 60 A, and
 Hardness of the second-generation rolling sensors = 60 D

(a) Hardness Chart of Polyurethane

Hardness	Tensile Modulus (PSI)			Tensile strength	Elongation at break	Tear resistance (lb./in.)			Compression set	Rebound
	100% elongation	200% elongation	300% elongation	(PSI)	(%)	Die C	Split	Trouser	(%)	(%)
63A	285		430	4320	760	195	42		51	
71A	300		500	5050	725	260		125	34	32
82A	375		1120	4500	585	345	100		35	21
91A	1100		2200	5500	430	600	90		30	42
50D	1800		4300	6500	380	700	130		36	40

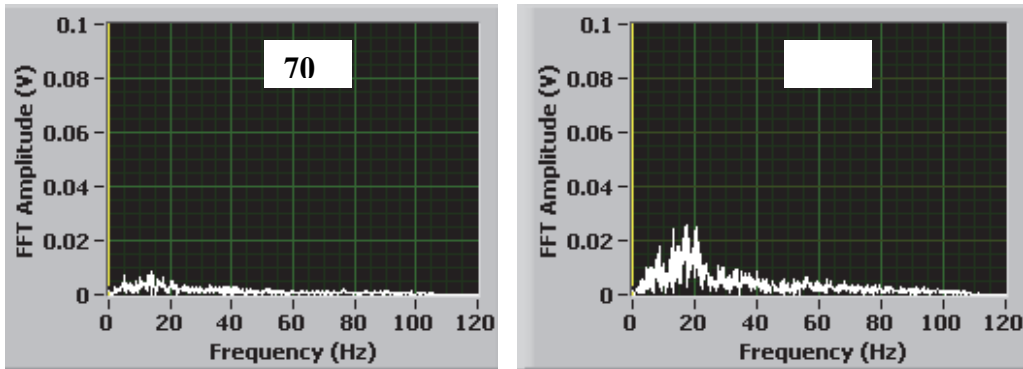
(b) Physical Properties of Urethane

Figure 3.7: Information of Urethane Hardness and Its Physical Properties (from PSI Urethane Inc. 2009)

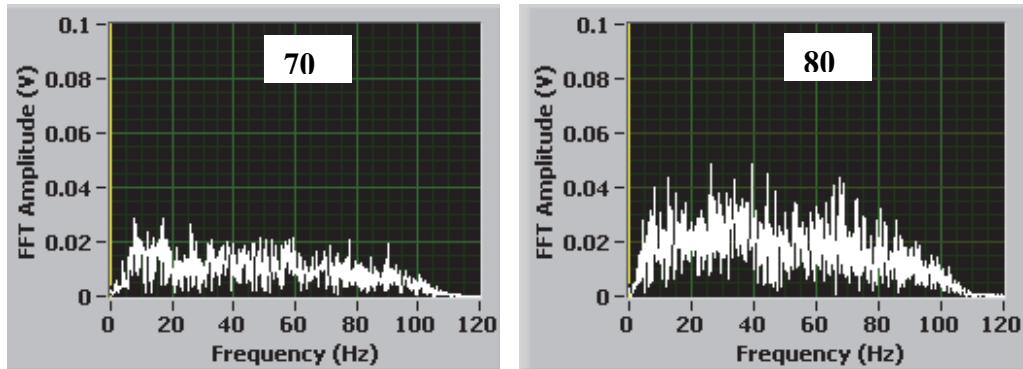
Before fabricating the CEM-design rolling sensors, the effect of stiffness of the urethane wheel tread was evaluated by using a two-wheel sensor system designed by Nam (Nam 2010). Nam’s rolling sensor is composed of two, 1-in. wide wheels and 2-Hz geophone located midway between the two wheels. With two sets of rolling sensors with urethane hardnesses of 70 A and 80 A, noise measurements at different speeds of 1, 3, and 5 mph (with no RDD dynamic loading) along the Pickle Research Campus (PRC) asphalt road were performed. FFT spectra with a linear scale are shown in Figure 3.8. Results with the softer urethane (70 A) exhibited lower rolling noise, especially around 30 Hz, a typical RDD operating frequency. Based on findings from this noise measurement and in consultation with PSI and CEM, the wheel-tread urethane with a 50-A durometer rating (pencil-eraser hardness) was selected for the final CEM-design rolling sensors. More studies on the rolling noise evaluation associated with the CEM-designed sensors are presented in Section 3.7.

The effect of the thickness of the urethane wheel tread was also evaluated. For this study, the research team fabricated one rolling sensor (second-generation rolling sensor with three wheels and a hold-down force) with the wheel tread urethane of 50 A. The dynamic response of the sensor was investigated by performing a field sensor calibration. The field calibration

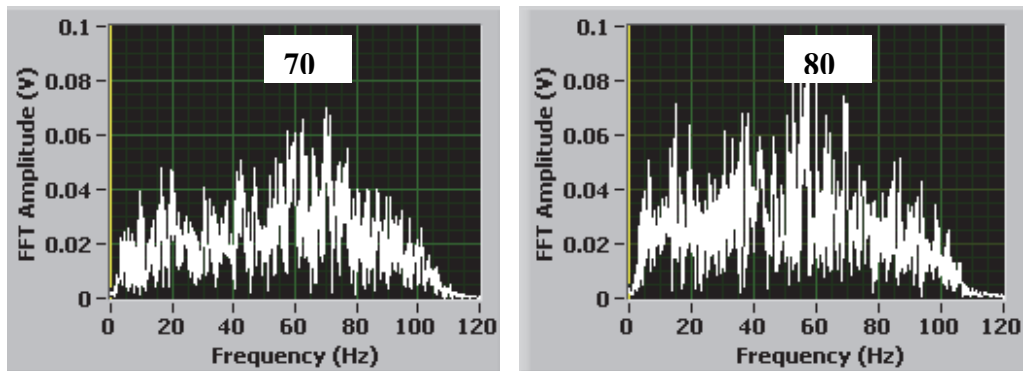
involves stationary testing of the sensor over a wide frequency range. The pavement motions are measured by fixing a small metal plate to the pavement surface using “fast-set” epoxy. The metal plate is located directly below the geophone on the rolling sensor. Once the metal plate is glued to the pavement, a calibrated reference transducer is screwed to this plate. A high-precision accelerometer (Wilcoxon 736T) was used as the transducer to measure the dynamic motion of the pavement surface. The RDD was then used to perform swept sine loading over a range of frequencies from 20 to 70 Hz.



(a) Speed of 1 mph; $f_s=512$ Hz



(b) Speed of 3 mph; $f_s=1536$ Hz



(c) Speed of 5 mph; $f_s=1536$ Hz

Figure 3.8: Noise Measurements (No RDD Dynamic Loading) Using a Two-Wheel Rolling Sensor with Wheel Tread Urethanes of 70A and 80A; Linear Spectra of a 5-second Measurement Window at Different Speeds of 1, 3, and 5 mph

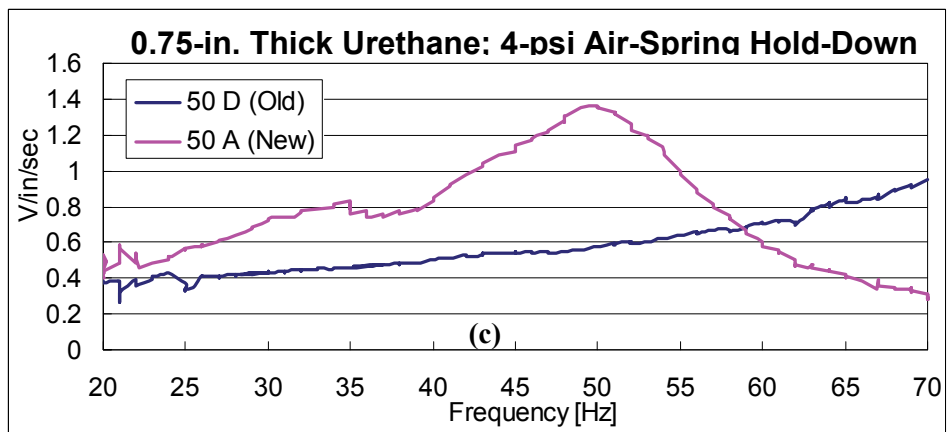
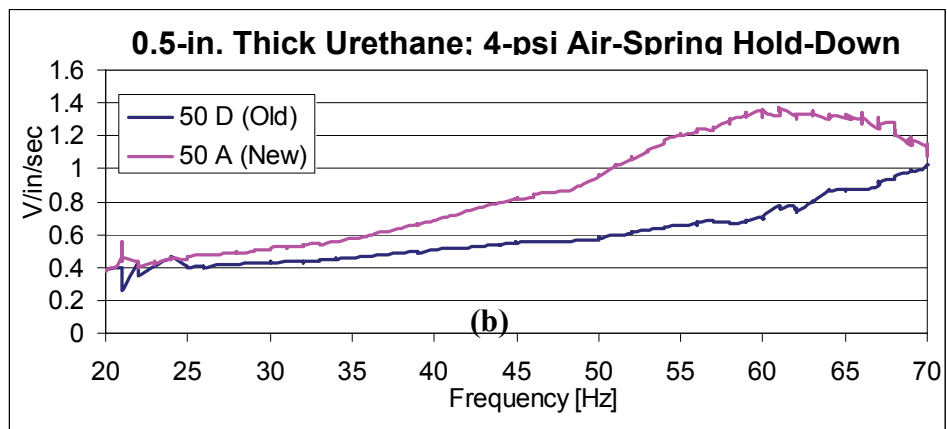
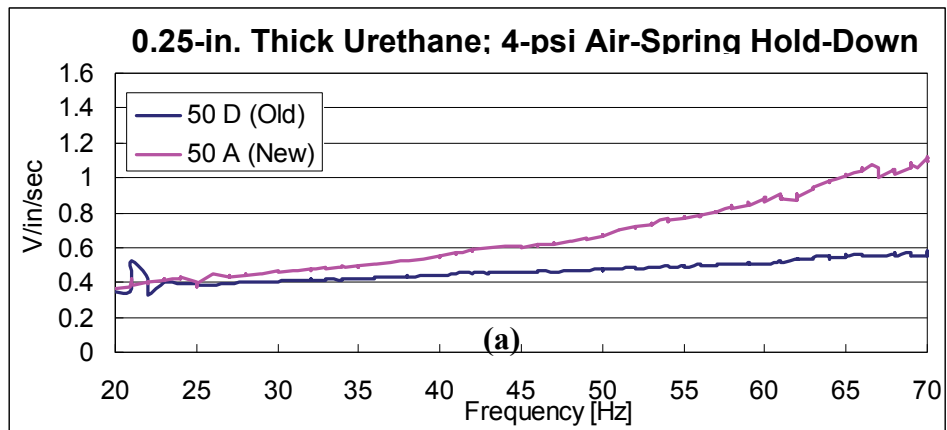
During the calibration process, urethane sheets (same hardness as 50 A) were placed under the three rolling wheels to vary the thickness of the urethane wheel tread. Three thicknesses of 0.25 in. (no urethane sheet), 0.5 in., and 0.75 in. were evaluated. For comparison purposes, the second-generation sensor that involves 50 D urethane was also calibrated at the same location.

The results of the field sensor calibrations are shown in Figure 3.9. In Figure 3.9, the sensor with 50 D is referred as the “Old Sensor” and the sensor with 50 A is referred as the “New Sensor.” During the sensor calibration, the same hold-down force of 4 psi in the air spring (see Figure 3.2b) was consistently used. During the sensor calibration with the 0.75-in. thick urethane tread shown in Figure 3.9c, air-pressure variations occurred in the frequency range of 25 to 40 Hz, resulting in the variations of sensor calibration factors. It is observed in Figure 3.9 that thicker wheel-tread urethane results in a softer sensor system and causes its resonance to move to lower frequencies. For the softer urethane (50 A) tread, the sensor with a 0.25-in. thick urethane tread does not show a resonance peak in the test range, while the sensor with a 0.75-in. thick urethane tread exhibits resonance around 50 Hz.

3.5.2 Sensor Hold-Down Force

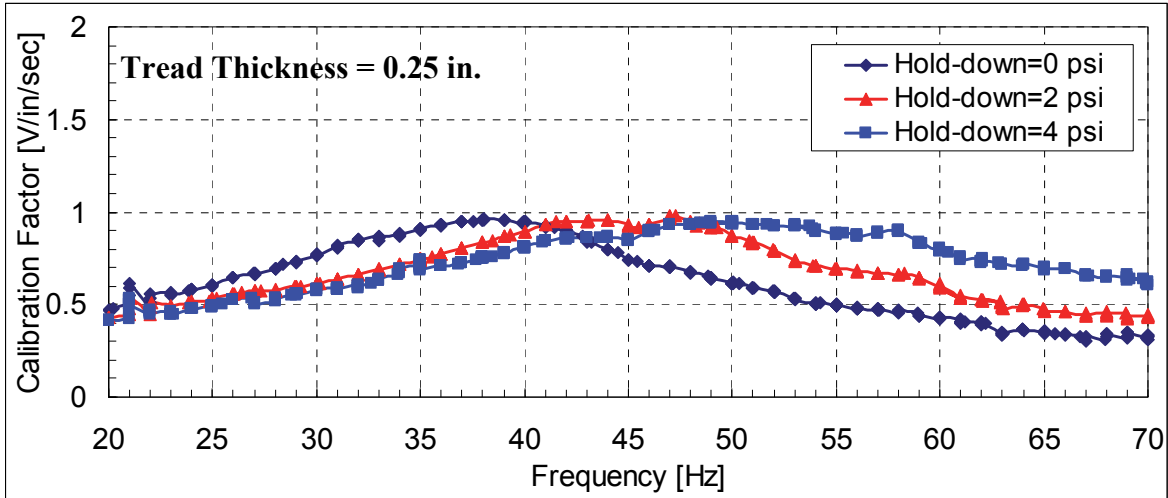
Sufficient hold-down force can maintain the rolling sensor in contact with the pavement surface at increased testing speeds. It was found that the air pressure inside an air spring (shown in Figure 3.2b) has no influence on the sensor calibration curve of the second-generation rolling sensors (Lee 2006). In other words, the amplitude of the sensor output voltage is not affected by variations of the hold-down force under RDD dynamic loading. The second-generation rolling sensor is composed of three, 9-in. diameter wheels coated with polyurethane 50 durometer on the D scale, which is golf-ball hardness. Due to this stiff urethane coating, the second-generation sensor exhibits no significant influence of hold-down force. However, the potential rolling sensors for the TPAD have more compliant wheel treads than the second-generation rolling sensor. Increasing the hold-down force thus compresses the compliant urethane and changes the stiffness of the urethane-tread-pavement contact.

To better understand how the pressure inside the air spring affects the sensor performance, field sensor calibrations under different levels of hold-down force (created by changing the pressure in the air spring) were performed. The sensor calibration involved the stationary RDD and the rolling sensor, placed at the position of Sensor #3 (shown in Figure 1.1b). Then, the RDD was used to apply a swept sine loading over a range of frequencies from 20 to 70 Hz. Different levels of sensor hold-down forces (expressed by pressures in the air spring of 0, 2, and 4 psi) were applied during the sensor calibration procedure. Unlike the second-generation rolling sensor that has stiff urethane tread (50 durometer in D scale), the level of the hold-down force has some influence on performance of the sensor with softer urethane (50 durometer in A scale) tread. The three sensor calibration curves under hold-down force from air-spring pressures of 0, 2, and 4 psi are shown in Figure 3.10. As shown in Figure 3.10, the resonance of the rolling sensor (urethane of 50 A) is changed by the level of hold-down force. When the hold-down force increases, the polyurethane coating compresses and increases the contact area between the wheel and the pavement, resulting in a stiffer system. The stiffer system increases the sensor resonant frequency. When the hold-down force decreases, the rolling sensor system becomes less stiff. As a result, the softer system (using softer polyurethane coating) lowers the sensor resonance frequencies.

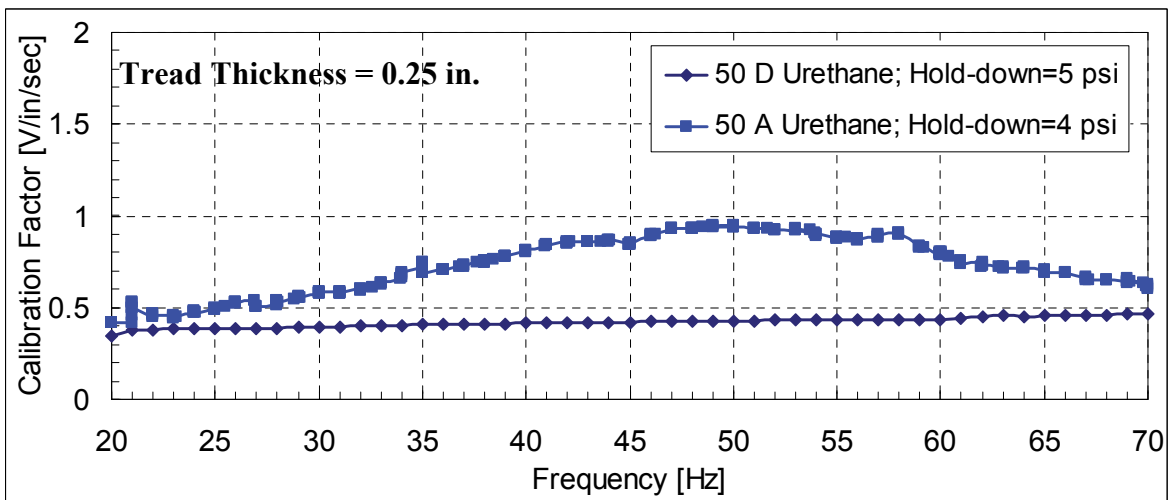


(Note: air-pressure variation during the calibration in the frequency range from 25 to 40 Hz)

Figure 3.9: Dynamic Response of a Rolling Sensor with Different Urethane-Tread Thicknesses: (a) 0.25-in. Thick Urethane, (b) 0.5-in. Thick Urethane, and (c) 0.75-in. Thick Urethane



(a) Sensor Calibration Curves under Different Hold-Down Forces



(b) Sensor Calibration Curves of Old RDD Sensors and TPAD Sensor

Figure 3.10: Field Sensor Calibration of the Second-Generation Sensor with a 50 A Urethane Tread: (a) Calibration Curves with Hold-Down Forces of 0, 2, and 4 psi and (b) Calibration Curves of the Sensor with 50 A and 50 D

3.6 Rolling Noise Measurement

3.6.1 Rolling Noise Characteristics and Signal-to-Noise Ratios

The Falling Weight Deflectometer (FWD) applies an impulsive force to a pavement by dropping weights from pre-defined heights. The typical duration of the FWD impulse load is about 30 ms and its predominant frequency is around 30 Hz. On the other hand, the RDD applies both static and dynamic forces on the pavement through two loading rollers. The dynamic force is a single-frequency sinusoidal force. The typical range in RDD operating frequencies is between 20 and 40 Hz. In this study, the RDD signal (dynamic component of pavement movement) is defined as the signal corresponding to the RDD operating frequency (f_0). Rolling

noise is defined as any frequency signal outside the RDD f_0 (see Figure 3.11a). (Rolling noise also exists in the RDD operating frequency.) This definition allows pavement deflections induced by the applied RDD dynamic loading to be distinguished from other sources of noise (i.e., rolling noise and traffic noise). As a result, rolling noise can be significantly filtered out by applying a proper signal processing technique such as a band-pass (notch-pass) digital filter as done by Bay, 1997.

The rolling sensors record pavement deflections (RDD signals) and rolling noise when RDD profiling is performed along the pavement. In contrast, no rolling noise is present when the RDD operates in a stationary mode. In the RDD data processing procedure, lower noise and a higher signal-to-noise ratio (SNR) allow more accurate deflection measurements. As shown in Figure 3.11b, the SNR is defined in this work as:

$$SNR = 20 \log_{10} \left(\frac{V_{RDD,30Hz}}{V_{20-40Hz}} \right) \quad (3.1)$$

where $V_{RDD,30Hz}$ = voltage measured at the RDD operating frequency (30 Hz), $V_{20-40Hz}$ = average voltage measured in the frequency band between 20 and 40 Hz (excluding the amplitude at 30 Hz) and the units are in decibels (dB).

It should be noted that V_{RDD} represents the signal at the operating frequency, assumed to be 30_{HZ}. However, for the example shown in Figure 3.11, the operating frequency is 35_{HZ}. With Equation 3.1, it can be seen that, if $V_{RDD, 35HZ}$ is 10 times $V_{20-40 Hz}$, then $SNR = 20dB$. Hence, 20 dB equals a factor of 10 difference in amplitudes. For the results presented in Figure 3.11b, the SNR of 30 dB represents a factor of about 32; hence, $V_{RDD 35HZ}$ is about 32 times larger than $V_{20-40 Hz}$. This presentation of SNR (Equation 3.1) is very common in signal processing.

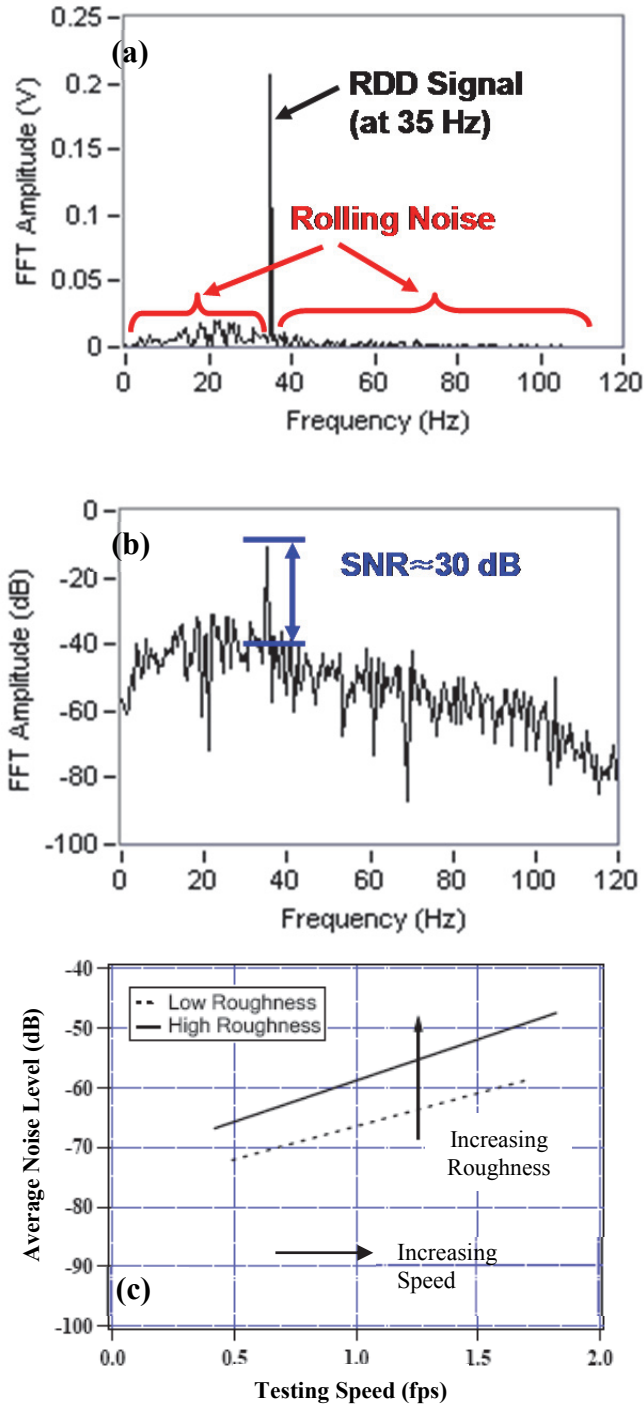


Figure 3.11: Rolling Noise Characteristics and Signal-to-Noise Ratio (SNR): (a) Rolling Noise Definition, (b) SNR Calculation, and (c) Generalized Relationship between Rolling Noise, Test Speed, and Pavement Surface Roughness (from Lee 2006)

For the larger wheels of the rolling sensors, the characteristics of the rolling noise and the SNRs are mainly determined by two factors: (1) testing speed and (2) pavement surface roughness. Each factor is not an independent input and can influence the others. The relationship

between each factor is illustrated in Figure 3.11c. The diagram shown in Figure 3.11c is a simplified observation based on previous RDD raw data.

3.6.2 Measurement of Continuous Noise-Level Deflection Profiles

Noise measurements using the second-generation sensor with wheel treads of urethanes 50 D and 50 A were performed at the speeds of 1, 3, and 5 mph along Path E at the TxDOT FSF. During these noise measurements, RDD testing with no dynamic loading and a sensor hold-down pressure of 5 psi (i.e., 95 lbs) was performed to obtain the noise-level deflection profile for only rolling noise and not noise induced by the RDD loading. The rolling sensor recorded only rolling noise while the RDD vehicle continuously moved along the pavement. To calculate the noise-level deflections, the raw data from the rolling sensor (which contained only rolling noise) were passed through a band-pass (or notch-pass) digital filter. The band-pass filter operates at the same frequency as the RDD (30 Hz in this study) and attenuates the other frequency components. The filtered noise signals are then plotted along the traveled distance. This procedure results in a noise-level deflection profile along the pavement. In other words, these noise-level deflections represent values that are so close in frequency to the RDD deflections that the band-pass filter cannot remove them. For instance, the band-pass frequency of 30 Hz in the filter is used to construct a 30-Hz noise-level deflection profile.

The noise-level deflection profiles collected at speeds of 1, 3, and 5 mph are shown in Figures 3.12, 3.13, and 3.14, respectively. In the titles and labels of these figures, the old sensor means the second-generation sensor with 50-D thread wheels and the new sensor is the second-generation sensor with 50 A. As illustrated in Figures 3.12 through 3.14, the rolling sensor with the softer urethane treads results in significantly lower noise-level deflections. The lower noise level with the new rolling sensor is mainly due to the softer urethane tread, which is less sensitive to the pavement surface. At a speed of 1 mph, the mean and σ for the old sensor are 0.32 and 0.17 mils, while the values for the new sensor are 0.10 and 0.07 mils. Several deflection peaks observed in the noise-level deflection profile of the old sensor at 3 mph (see Figure 3.13) are most likely due to sensor decoupling at joints involving wide openings. At a speed of 3 mph, the mean and σ for the old sensor are 1.77 and 0.90 mils while the values for the new sensor are 0.60 and 0.52 mils.

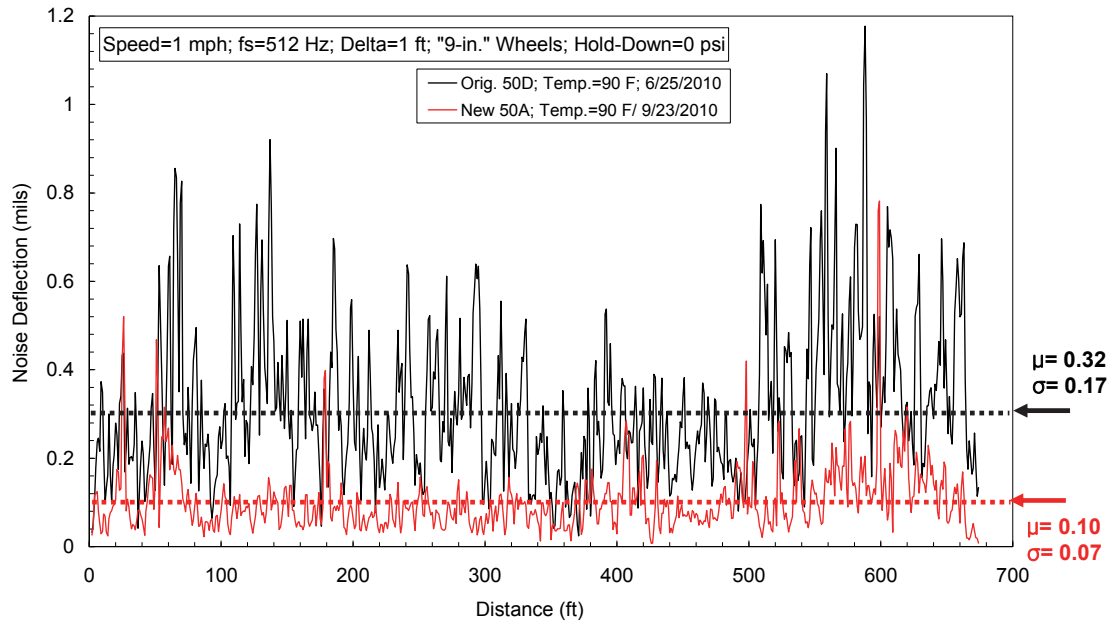


Figure 3.12: Noise-Level Deflection Profiles at 1 mph Using the Second-Generation Old and New Rolling Sensors Collected along Path E at the TxDOT FSF

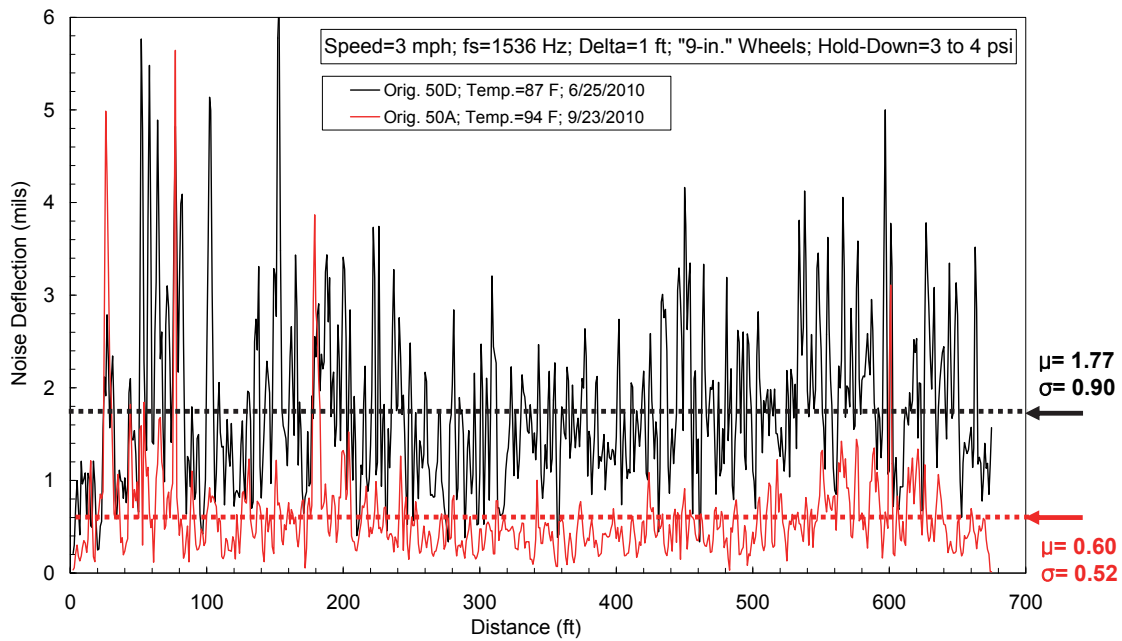


Figure 3.13: Noise-Level Deflection Profiles at 3 mph Using the Second-Generation Old and New Rolling Sensors Collected along Path E at the TxDOT FSF

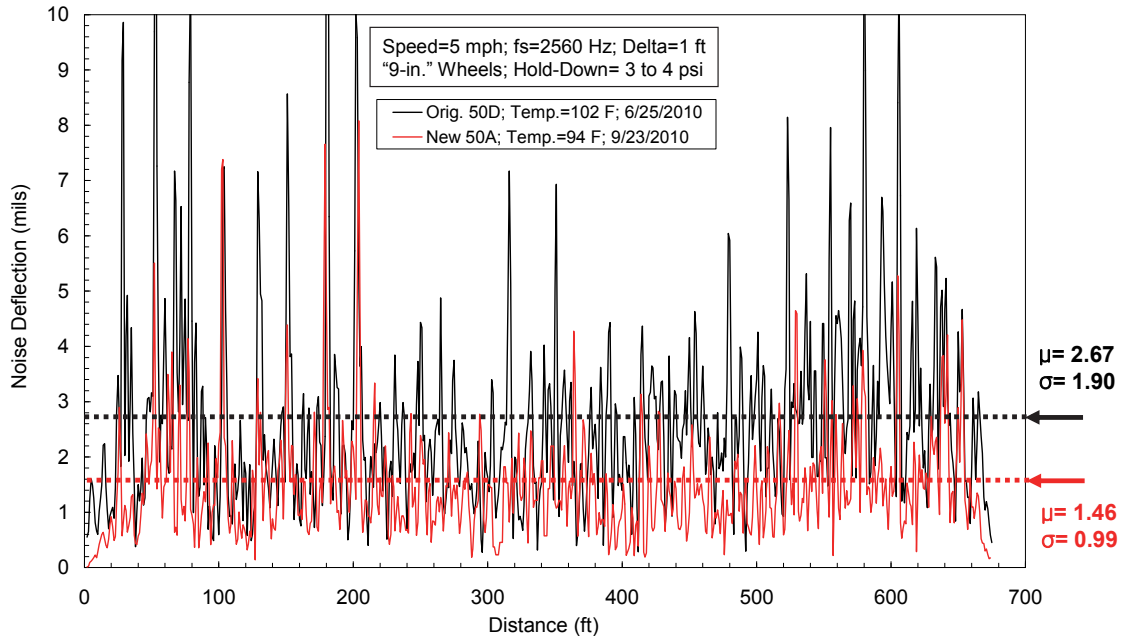


Figure 3.14: Noise-Level Deflection Profiles at 5 mph Using the Second-Generation Old and New Rolling Sensors Collected along Path E at the TxDOT FSF

Several general observations made from these results are the following. First, noise-level deflections increase with increasing testing speed. Second, joints cause higher rolling noise than mid-slab areas at the same rolling speed. Lastly, joints on the 16-in. thick slabs, which have wider joint openings, caused higher levels of rolling noise than joints on the 8-in. thick slabs at the TxDOT FSF. The 16-in. thick slabs are 25 ft long and 25 ft wide. These slabs have wider joint openings than the 8-in. thick slabs, which results in a higher level of rolling noise especially at the higher testing speeds of 3 to 5 mph. The width of joint openings is a critical parameter controlling the noise level, especially for the higher testing speeds of 3 to 5 mph. The average noise-level joint deflection over all 16-in. thick slabs is less than 2 mils, while the average joint deflection over all 8-in. thick slabs is approximately 4 mils. Considering the levels of joint deflections, the noise level shown in Figures 3.13 and 3.14 are very significant because the noise level can be higher than the RDD signal. Therefore, improved signal process to account for rolling noise needs to be done in future work.

3.7 Deflection Measurements

A preliminary study to investigate temperature effects on the RDD deflection measurement was performed at the TxDOT FSF. The original RDD was used to profile Path E at different pavement surface temperatures. As the pavement surface temperature increases, the deflections at joints significantly decrease while the deflections in the mid-slab areas slightly increase (Nam 2010). This observation can be explained by the combination of slab curling and slab expansion with increasing pavement temperature. To minimize the adverse impact of temperature increase in this work dealing with comparing second-generation and new rolling sensors, field tests with the original RDD were performed between 7:00 a.m. and 10:00 a.m. when the pavement surface temperature was less than about 100 °F (38 °C). Also, this study

began near the end of Year 1, continued into Year 2, and was completed in the first month of Year 3. Even though, the work covered about 15 months, it is reported herein for completeness.

Continuous RDD profiling along Path E using the new rolling sensors was performed at average test speeds of 1, 3, and 5 mph. The rate of sampling the rolling sensor output was increased from 256 Hz to 512 Hz at 1 mph. During testing at other speeds, the sampling rate was proportionately increased as the rolling speed increased. The deflection profiles collected at the average test speeds of 1, 3, and 5 mph are shown in Figures 3.15, 3.16, and 3.17, respectively. It is observed that the deflection profiles evaluated at 1 and 3 mph show very similar results, with the exception of deflections at some joints, mainly for the 16-in. thick slabs (see Figure 3.16). The deflection profile at the 5-mph speed shows noisier signals. However, a reasonable comparison between the deflection profiles measured at 1 and 5 mph still exists, except for the 16-in. thick slabs at joints (see Figure 3.17). These differences observed in the 16-in. thick slabs are mainly due to the high level of rolling noise at the joints.

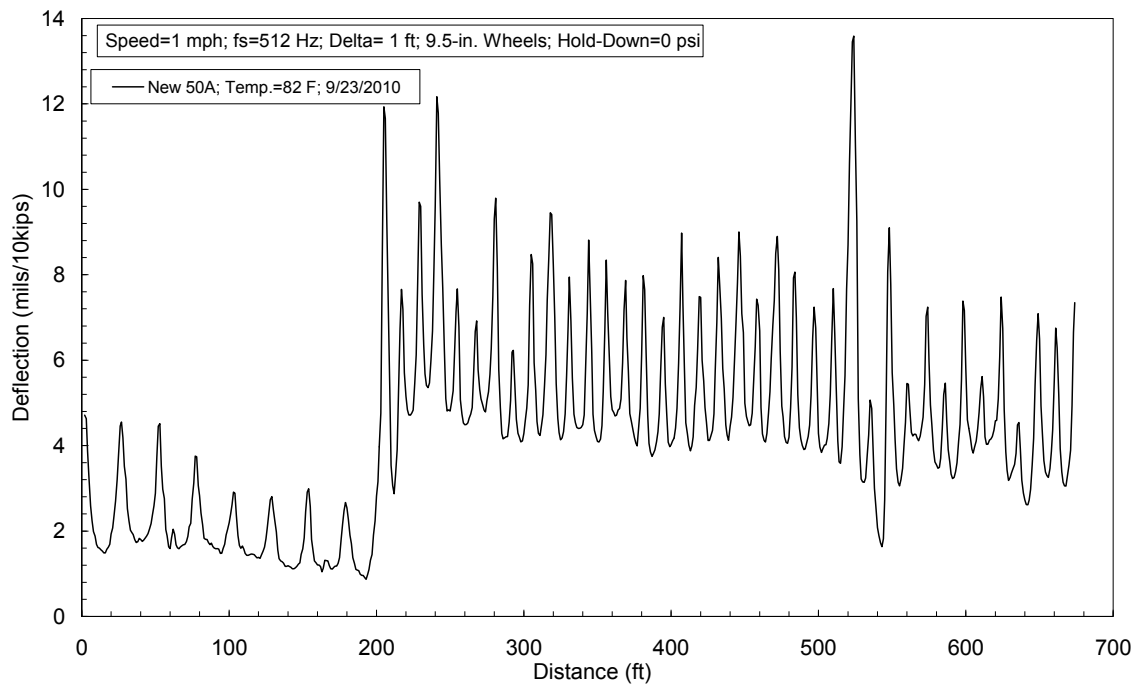


Figure 3.15: Continuous Deflection Profile at 1 mph Using the New Rolling Sensor along Path E at the TxDOT FSF

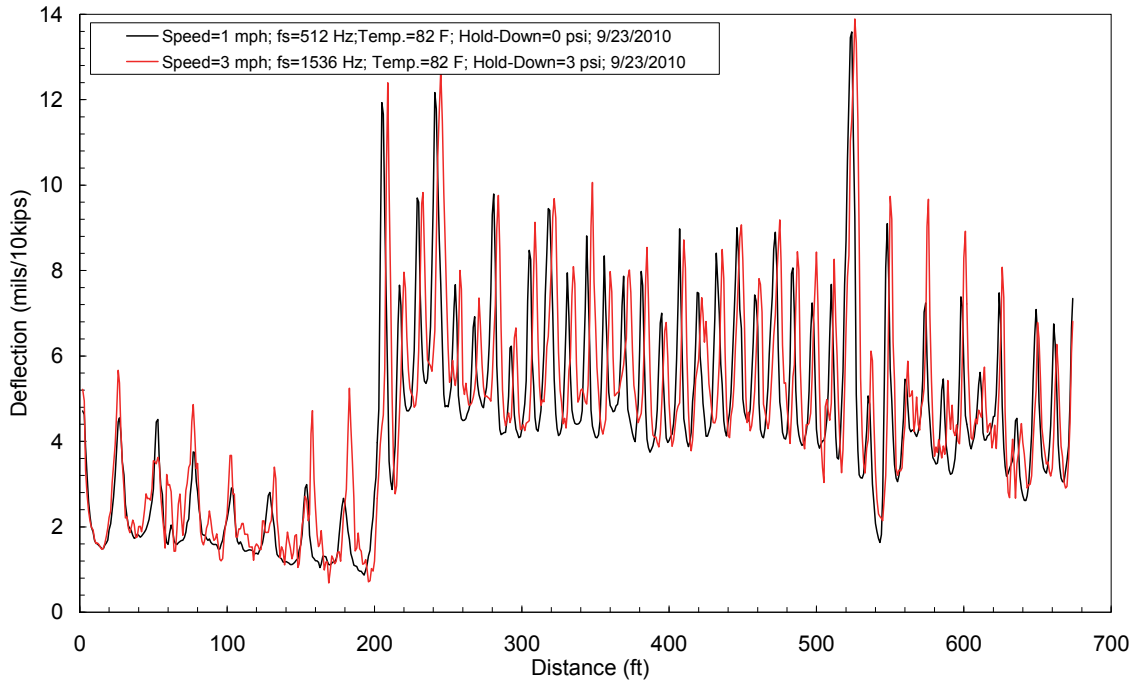


Figure 3.16: Continuous Deflection Profiles at 1 and 3 mph Using the New Rolling Sensor along Path E at the TxDOT FSF

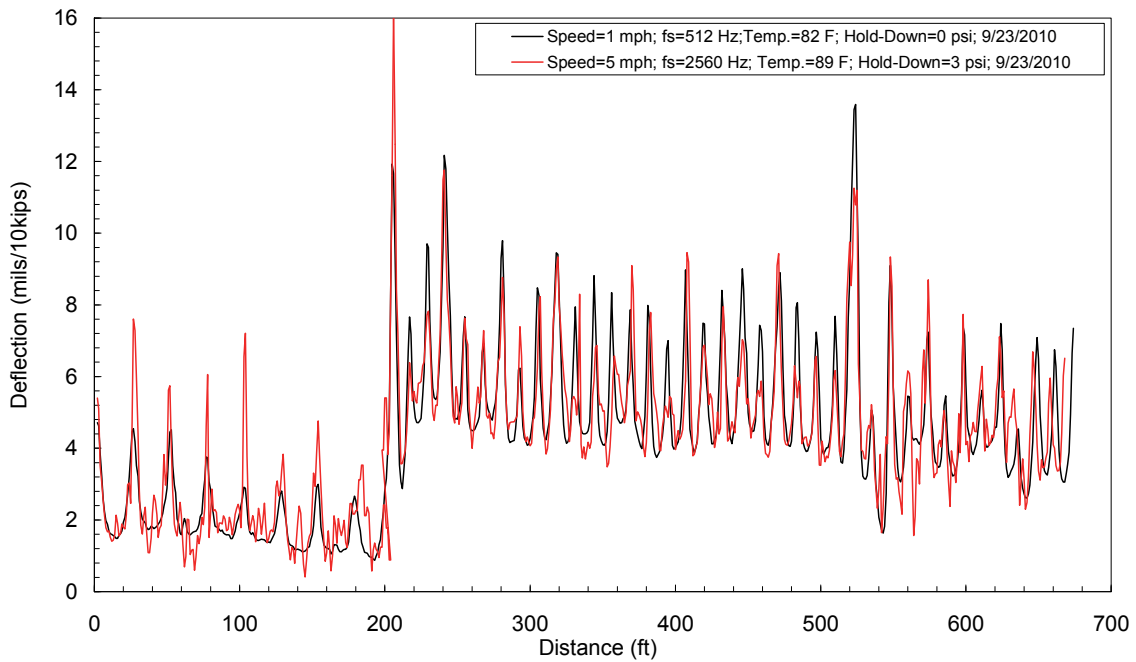


Figure 3.17: Continuous Deflection Profiles at 1 and 5 mph Using the New Rolling Sensor along Path E at the TxDOT FSF

The deflection profiles at 1, 3, and 5 mph using the old rolling sensor and the second-generation rolling sensor with 9-in. diameter wheels with wheel treads of 50-D urethane were also measured to compare with the deflection profiles measured with the new sensor. Testing dates for RDD testing with the second-generation (Lee, 2006) and new sensors were July 2009 and September 2010 for one set of comparisons, and June 2010 and September 2010, for the second set of comparisons. Testing times were between 7:00 a.m. and 10:00 a.m. before the JCP slabs change their behavior due to the pavement temperature change. Deflection profiles collected using the old and new sensors at speeds of 1, 3, and 5 mph are compared in Figures 3.18, 3.19, and 3.20, respectively. As observed in Figure 3.18, different testing dates seem to have caused slight differences in the joint deflections between the two deflection profiles. In the deflection profiles at 1 mph, the new sensor results in less noisy signals than the old sensor. As the test speed increases, the old sensor apparently shows higher rolling noise than the new sensor. In the deflection profiles at 5 mph, the old sensor does not show a clear pattern of mid-slab and joint deflections along Path E. Based on these observations, it is concluded that more compliant urethane threads generate lower rolling noise and better contact with the pavement at higher test speeds. The recommendation at this time is that 50-A tread urethane with 0.75 in. in thickness be used for the final TPAD rolling sensor.

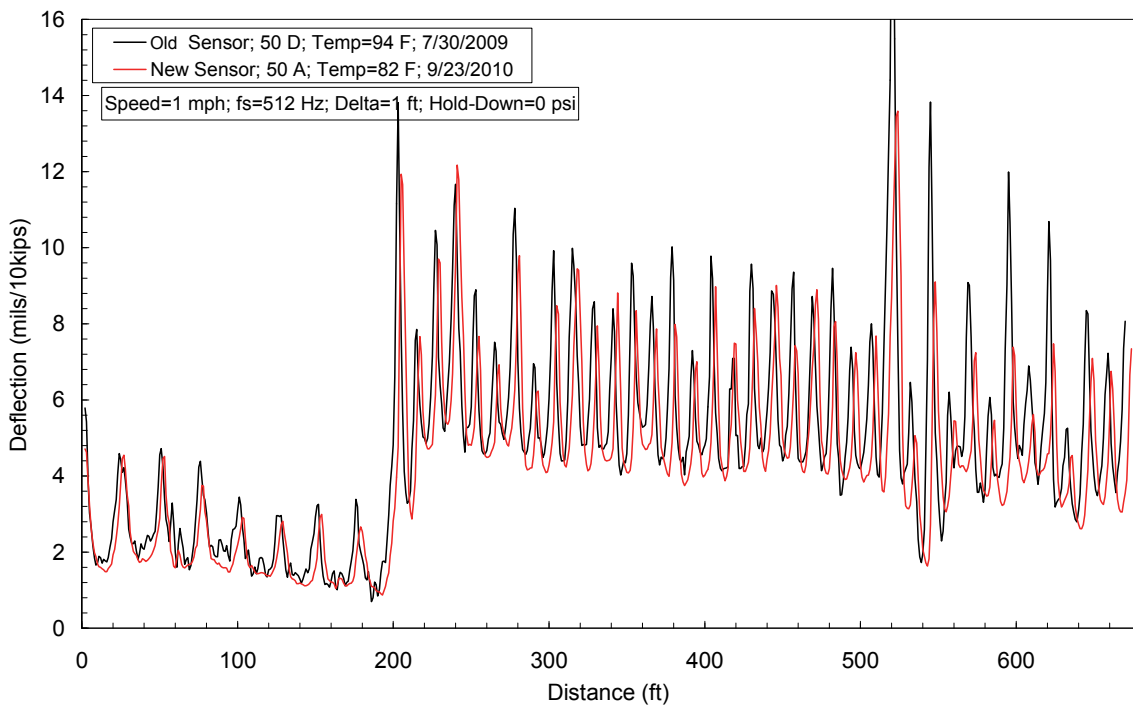


Figure 3.18: Continuous Deflection Profiles at 1 mph Using the Old and New Rolling Sensors Collected along Path E at the TxDOT FSF

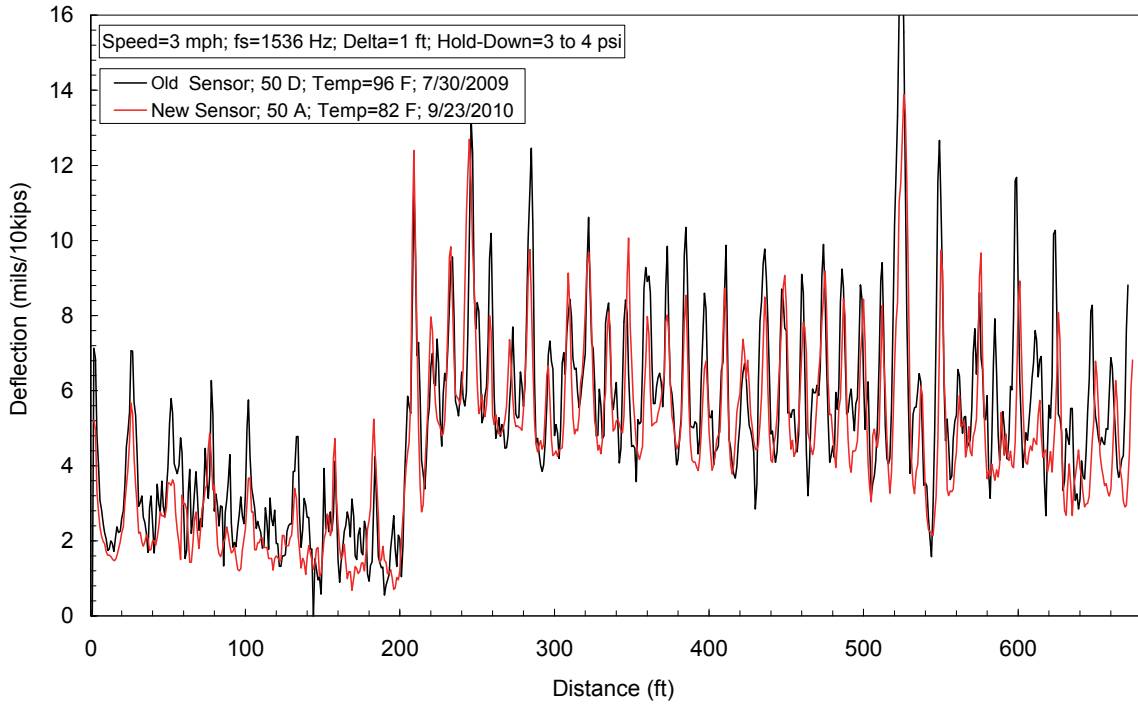


Figure 3.19: Continuous Deflection Profiles at 3 mph Using the Old and New Rolling Sensors Collected along Path E at the TxDOT FSF

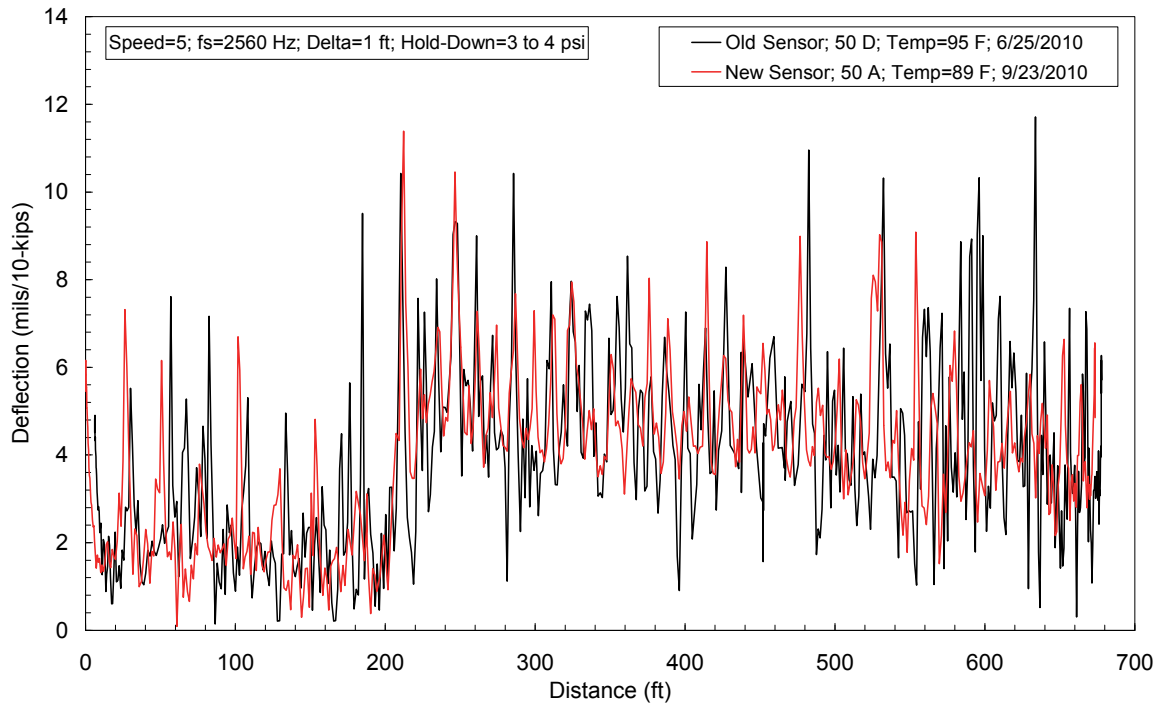


Figure 3.20: Continuous Deflection Profiles at 5 mph Using the Old and New Rolling Sensors Collected along Path E at the TxDOT FSF

Chapter 4. Improvements to the RDD Data Analysis Procedure

4.1 Introduction

The primary advantage of the RDD is that it continuously measures pavement deflections as the vehicle moves along a pavement. When compared with a device such as the Falling Weight Deflectometer (FWD) that is used to test at discrete points, the RDD has a more complex data analysis procedure. The FWD drops a weight from a known height and generates a dynamic impulsive force. This impulsive force is applied to the pavement through a circular loading plate. Then, geophone sensors at multiple locations measure the velocity of the pavement surface due to the impulsive load. The maximum deflections measured at each geophone are calculated and combined to obtain a deflection basin. The geophone used in FWD testing is a velocity transducer that outputs voltage signals proportional to the measured pavement-surface velocity. The geophone uses the acceleration of gravity as the reference so it only measures the dynamic component of the pavement motion.

On the other hand, the RDD applies a single-frequency sinusoidal dynamic force to the pavement surface. The dynamic force is applied to the pavement through two loading rollers, and the pavement is vibrated by the operating frequency of the RDD. Then, the rolling sensors are used to record the induced pavement deflections at multiple locations and, due to the nature of the contact-type sensor, the rolling noise. The RDD signal processing is a robust technique because it allows the separation of the RDD signals from much of the rolling noise in the frequency domain. The band-pass (or notch-pass) digital filter is then used to remove rolling noise components from the RDD deflection signals.

In the first part of this chapter, a review of the current RDD signal processing analysis is presented and the limitations of the current analysis algorithm are discussed. In the second part of the chapter, an alternative scheme to improve the current data processing technique is presented.

4.2 Original RDD Data Analysis

4.2.1 Overview of the Original Data Processing

The original technique of data processing used in RDD testing was designed for the first-generation rolling sensor that consists of three, 6-in. diameter wheels. Measurements of RDD raw data are composed of three groups: (1) force measurements from four load cells, (2) dynamic deflection measurements from multiple rolling sensors, and (3) distance measurements from the distance encoder. The signal processing technique is applied to all three measurements to remove rolling noise which is considered to be noise signals outside the RDD operating frequency. By selecting an appropriate filtering scheme, it is relatively easy for the force signals due to their high SNRs (typical SNR is about 70 to 80 dB). In contrast, the rolling sensor outputs have much lower SNRs (typical SNR is about 20 to 30 dB) than the force signals. Therefore, the digital filter was designed mainly for treating the signals measured by the rolling sensors. Details of RDD data processing can be seen in Bay and Stokoe (1998). A brief overview of RDD data processing is presented below.

RDD data processing is similar to the demodulation operation of an amplitude modulation (AM) radio receiver. In the procedure of AM radio transmission, the magnitude, $f(t)$, and phase, $\Phi(t)$, of the audio transmission are first modulated. The signal modulation means that

the AM radio transmitter takes an acoustic signal and multiplies the signal by a radio frequency carrier signal. This modulation technology allows the radio signal to transmit further with less signal degradation. When the radio signal arrives at the AM radio receiver, the audio transmission can be retrieved through the amplitude demodulation procedure on the signal. The amplitude demodulation and signal amplification are usually made by analog electronic circuits inside a radio receiver.

The numerical algorithm used in the procedure of RDD data processing is presented below. This numerical algorithm is used for both deflection and force measurements. The RDD signal can be represented as:

$$g(t) = f(t) \cos(w_o t - \phi(t)) + n(t) \quad (4.1)$$

where $g(t)$ = RDD displacement signals,

$f(t)$ = continuous displacement signal amplitude with time,

$\phi(t)$ = continuous phase of displacement signal with time,

w_o = RDD operating frequency, and

$n(t)$ = rolling noise with time.

The goal of RDD data processing is to retrieve the continuous displacement, $f(t)$, from the combined RDD signal and rolling noise signal, $g(t)$. In the demodulation procedure, the noise term, $n(t)$, is neglected and added back into the analysis later. Then, the function of $g(t)$ can be transformed into two new functions, $a(t)$ and $b(t)$, as:

$$f(t) \cos(w_o t - \phi(t)) = a(t) \cos w_o t + b(t) \sin w_o t \quad (4.2)$$

$$\text{where } f(t) = \sqrt{a^2(t) + b^2(t)} \text{ and } \phi(t) = \arctan \frac{b(t)}{a(t)}.$$

The first step in demodulation is to multiply the modulated function (Eq. 4.2) by the complex function below:

$$(\cos w_c t + i \sin w_c t)$$

where w_c is the carrier frequency, and $i = \sqrt{-1}$.

Neglecting noise in RDD signals, this multiplication can be described as follows:

$$\begin{aligned} & (f(t) \sin(w_o t - \phi(t)))(\cos w_o t + i \sin w_o t) = \\ & (a(t) \cos w_o t + b(t) \sin w_o t)(\cos w_o t + i \sin w_o t) = \\ & \frac{1}{2} a(t) + \frac{1}{2} a(t) \cos 2w_o t + \frac{1}{2} i a(t) \sin 2w_o t + \\ & \frac{1}{2} b(t) \sin 2w_o t + \frac{1}{2} i b(t) - \frac{1}{2} i b(t) \cos 2w_o t \end{aligned} \quad (4.3)$$

The product of this multiplication can be separated into two parts. The first part is the functions $a(t)$ and $b(t)$ times a constant, which is the DC term (i.e., 0 Hz). The second part is the functions $a(t)$ and $b(t)$ multiplied by sinusoidal functions with a frequency of $2\omega_0$, which is the AC term. The DC term has half the magnitude as the original audio transmission. The product of Eq. 4.3 can be filtered to recover the functions $a(t)$ and $b(t)$ from the product in Eq. 4.2. The filter needs to reject terms with the frequency $2\omega_0$. The filter design is a critical part of the demodulation procedure, and a low-pass filter with a cut-off frequency less than $2\omega_0$ can work as:

$$2 \left[\frac{1}{2} a(t) + \frac{1}{2} a(t) \cos 2\omega_0 t + \frac{1}{2} i a(t) \sin 2\omega_0 t + \frac{1}{2} b(t) \sin 2\omega_0 t + \frac{1}{2} i b(t) - \frac{1}{2} i b(t) \cos 2\omega_0 t \right] \xrightarrow{L-P} a(t) + b i(t) \quad (4.4)$$

where $\xrightarrow{L-P}$ represents filtering procedure using a low-pass filter.

Once the functions $a(t)$ and $b(t)$ are obtained after filtering, the amplitude and phase functions, $f(t)$ and $\phi(t)$, can be calculated using the following equations:

$$f(t) = \sqrt{a^2(t) + b^2(t)} \quad (4.5)$$

$$\phi(t) = \arctan \frac{b(t)}{a(t)} \quad (4.6)$$

The flow chart of the original RDD data processing is shown in Figure 4.1. During RDD testing, the rolling sensors record dynamic displacements of pavements in terms of voltages generated by the 2-Hz geophones. These voltages are digitized-voltage signals with a selected sampling rate, fs. The raw data recorded by each geophone are first multiplied by a complex function, which is an amplitude demodulation method. The complex demodulation product is filtered by a digital notch-pass filter. The filtered complex time series are then multiplied by rolling sensor calibration factors. Each rolling sensor—Sensors #1, #2, #3, and #4—has its own frequency-dependent calibration factor determined in the laboratory. The calibrated time series (velocity values) are converted to dynamic displacements that are averaged over a 1- or 2-sec time interval. To minimize the deflection variations due to dynamic loading variations while rolling, the displacements are normalized by a normalization force (typically 10 kips) for highway projects. This technique is a time-based method in which RDD deflections are reported based on a selected time interval (t90). The speed variation can have significant influence on this time-based method because it determines the spatial resolution. For instance, higher testing speeds result in lower spatial resolution while slower speeds result in better spatial resolution.

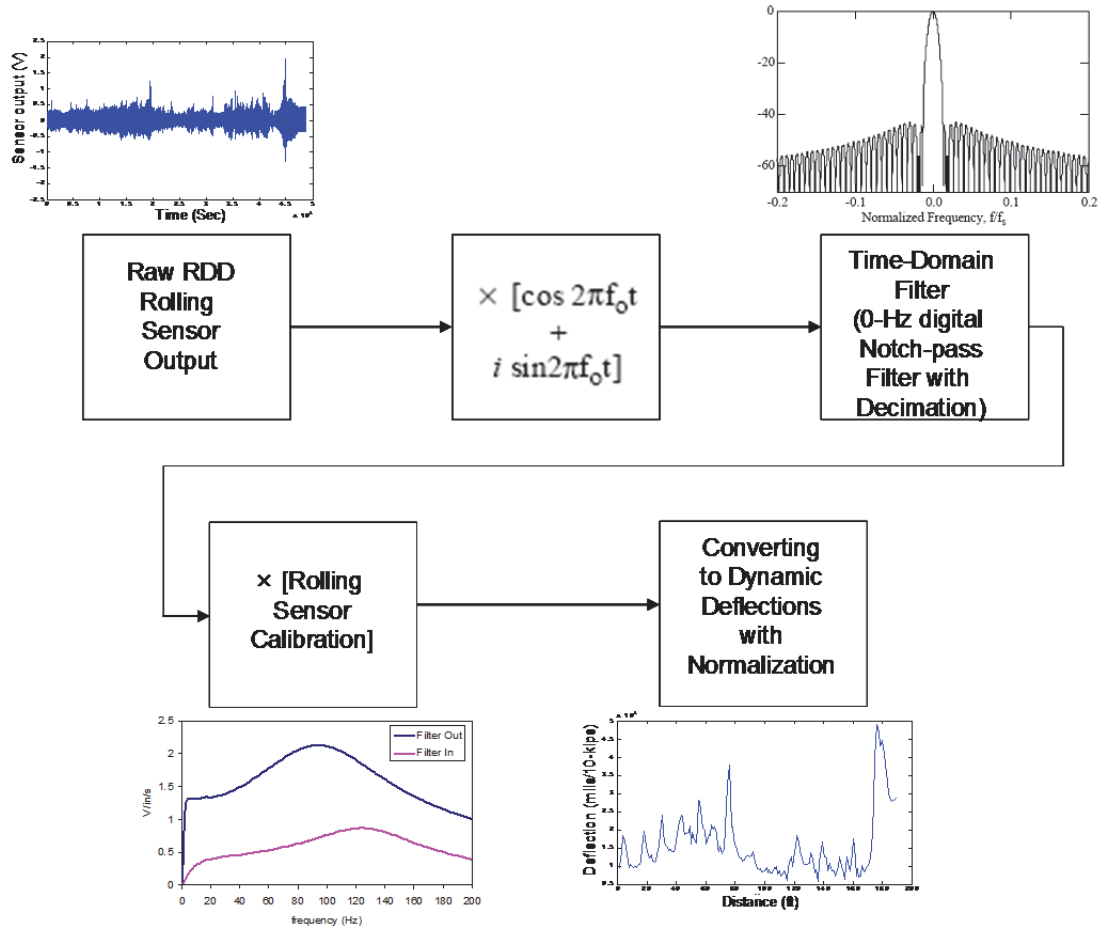


Figure 4.1: Flow Chart of Original RDD Data Processing to Calculate Dynamic Displacement versus Distance from the RDD Sensor Outputs

4.2.2 Limitations of the Original RDD Data Processing

The original data processing was designed for the first-generation (6-in. diameter wheels) rolling sensors for which the test speed is 1 mph or less. The original data processing technique utilizing the composite IIR and FIR filters has been successfully used to post-process RDD raw data over the past decade. However, this data processing technique has revealed several limitations. The original data processing technique utilizes a time-based analysis that reports average deflections computed over a selected time interval (typically 1 or 2 sec). The limitations of time-based analysis are summarized as below.

1. In the current RDD system, no technique has been used to maintain a constant testing speed other than the vehicle driver. Despite an effort to keep the test speed constant, test speed varies during testing. This speed variation causes variations in spatial resolution in a continuous deflection profile.
2. The typical time interval of 1 to 2 seconds leads to about a 1- to 3-ft (0.3 to 0.9-m) distance interval over which the average deflection is determined. Speed increases near cracks/joints may cause critical data points to be missed. This problem will be more significant at higher test speeds.

3. The original data analysis underestimates joint movements due to the nature of average deflections processed over a given time/distance interval. The time-based analysis provides an additional underestimation because the distance interval for a given time interval does not consider the same portions of adjacent slabs if the distance-interval position is biased to either side of the slabs.
4. For a JCP, the time-based method presents difficulties in locating the positions of the rolling sensors at joints. Sensors #1 and #2 should be positioned with equal distance from the joint (Sensor #1 is on the loaded slab and Sensor #2 is across the joint). Inappropriate positioning of Sensors #1 and #2 results in inappropriate load-transfer efficiency (LTE) values.

Based on the limitations above, we have concluded that the interval-sampling RDD deflections should be user-defined in a distance mode, not in a time mode. This approach is referred to as a distance-based method. In addition, the spatial resolution with this approach should be improved at higher testing speeds of 3 to 5 mph (4.8 to 8.0 km/hr) compared to the original approach.

4.3 Improved Data Analysis Procedure

4.3.1 Distance-Based Analysis

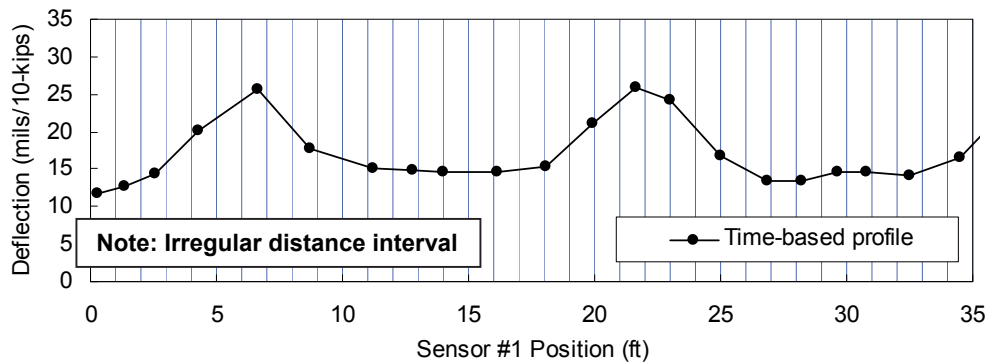
The improved data processing procedure is capable of constructing a distance-based deflection profile of which the spatial resolution is less affected by the variation of testing speed. One major limitation of the time-based method (old data processing scheme) is that the typical time interval of 1 to 2 seconds has the potential to miss critical cracks/joints because the speed increase results in lower spatial resolution. In this section, the procedure to construct the distance-based deflection profile is presented. In comparison to the old data processing procedure, three additional modifications are added in the data processing procedure as outlined below.

- (1) Increase the sampling rate during RDD data collection at all testing speeds. In the data processing procedure, the band-pass digital filter is applied to RDD raw data (rolling sensor outputs) to attenuate rolling noise. The filter bandwidth can also be adjusted depending on the level of rolling noise.
- (2) Select a desired distance interval (spatial resolution) for the RDD deflection profile. If a higher signal-to-noise ratio (SNR) is obtained during RDD data collection, a shorter spatial resolution can be used. In our experience, the distance interval of 1 ft provides a sufficient resolution in evaluating a jointed concrete pavement (JCP).
- (3) Average the data filtered with 0-Hz digital notch-pass filter over the distance selected according to SNR (the distance-based deflection profile).

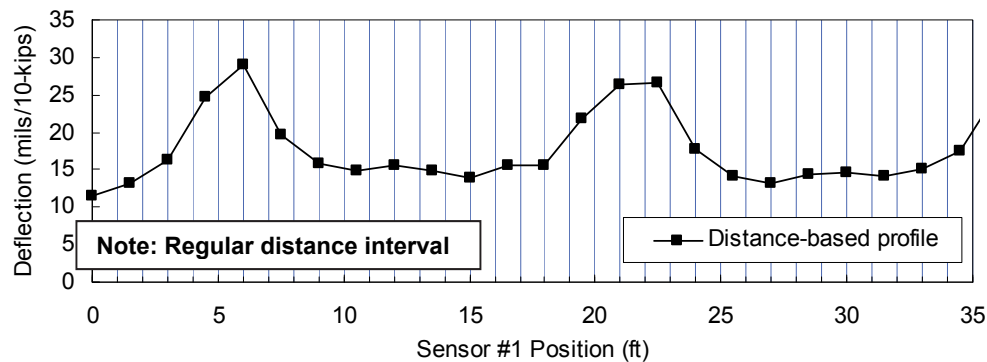
Unlike the time-based method, the number of data points to average, N_{avg} , over the same distance interval varies for each distance interval. A comparison of the time- and distance-based deflection profiles is shown in Figure 4.2. The data set collected along a JCP at the TxDOT FSF site using the first-generation rolling sensor at a speed of 1 mph were treated with the time- and distance-based methods. In the procedure of data processing, the time-based method used the

typical time interval of 1 sec while the distance-based method used a distance interval of 1.5 ft. The uniform spacing in data points in the profile evaluated with the distance-based profiling is clearly seen in Figure 4.2b. The improved deflection measurement at joints is shown at a distance of 6 ft in the figure.

In the distance-based deflection profile, the distance interval is user-defined. The level of rolling noise along a test path determines the spatial resolution. The distance-based deflection profiles with various spatial resolutions of 1, 1.5, and 2 ft are shown in Figure 4.3. It is observed that the deflection levels and the joint positions are slightly different for each profile. These differences are unavoidable because the data processing considers different positions in the distance intervals over which the raw data collected are processed and also different numbers of data points are averaged (N_{avg}). Clearly, the 1-ft distance interval presents a well-defined profile.

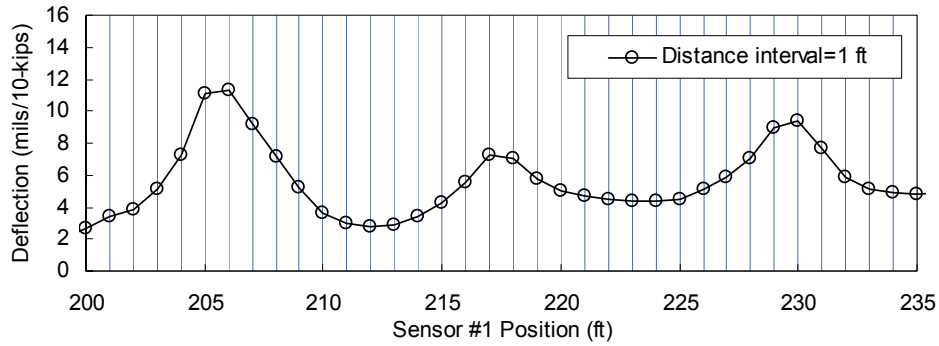


(a)

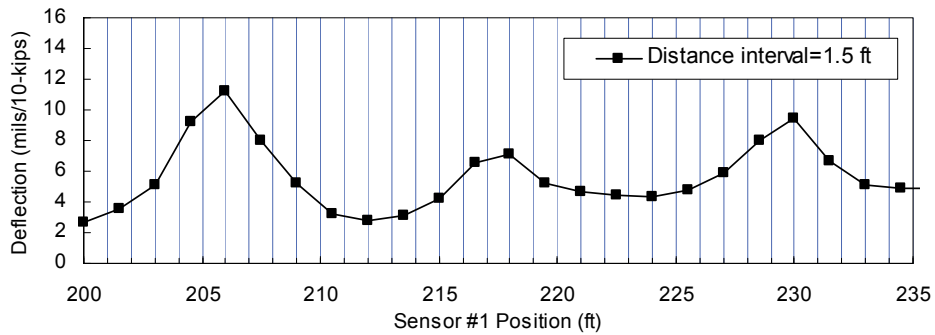


(b)

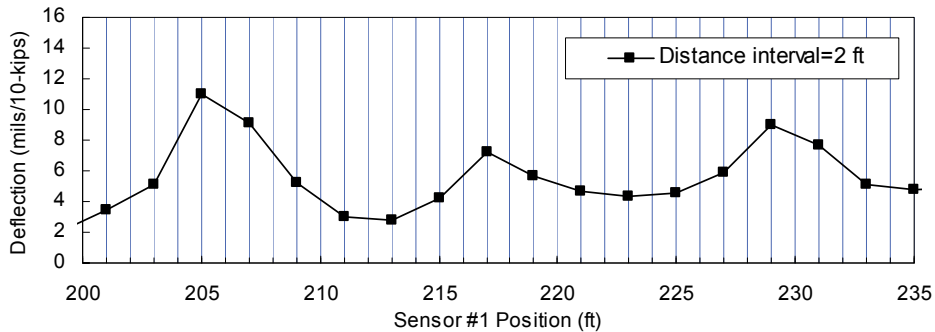
Figure 4.2: Deflection Profiles Constructed by Time- and Distance-Based Methods; Data Set Collected along a JCP Using the First-Generation Rolling Sensor (Sensor #1) at 1 mph: (a) Time-Based Deflection Profile with Time Interval of 1 sec and (b) Distance-Based Deflection Profile with Distance Interval of 1.5 ft



(a) 1-ft Distance Interval



(b) 1.5-ft Distance Interval



(c) 2-ft Distance Interval

Figure 4.3: RDD Distance-Based Deflection Profiles with Different Spatial Resolutions of 1, 1.5, and 2 ft; Data Set Collected along a JCP Using the First-Generation Rolling Sensor (Sensor #1) at 1 mph

4.3.2 Distance-Based Analysis with Moving Average

With the first-generation rolling sensors designed to be tested at 1 mph, the distance-based method allows a distance interval in the range of 0.5 to 3.0 ft, depending on the level of rolling noise. However, this distance-based method may not be sufficient for the speed-improved rolling sensor because higher levels of rolling noise due to higher test speeds require narrower filter bandwidths (BW_{20}). The narrower BW_{20} leads to longer filter settling time (t_{90}). Thus, a sufficiently long distance interval is necessary to maintain reasonable BW_{20} values for the speed-

improved rolling sensors of which the target speed is 5 mph or more. In this section, a new deflection-reporting method is proposed to improve or maintain the spatial resolution without sacrificing the performance of the digital filter (noise attenuation by the notch-pass digital filter) at higher test speeds.

The new method is to construct a moving average distance-based deflection profile (simply referred as a moving average profile). The moving average profile means that the distance interval over which the raw data is processed using the time-based analysis moves continuously along a test path with a selected distance increment (delta, Δ). In the moving average profile, two adjacent distance intervals have an overlapped area which is the distance interval minus the delta (Δ). For example, a distance interval of 2 ft is continuously sampled and moved with a distance increment of 1 ft. Hence the overlapped distance between two adjacent distance intervals is 1 ft. If a distance interval of 3 ft and a delta of 1 ft are used, the overlapped distance is 2 ft. As the distance interval approaches a joint, the maximum deflection occurs when the center of the distance interval is positioned at the joint (equally spaced on adjacent slabs). A graphical explanation of constructing the moving average profile is presented in Figure 4.4. In Figure 4.4, the distance interval is 2 ft and the delta is 1 ft, which gives moving average deflections at 1 ft intervals.

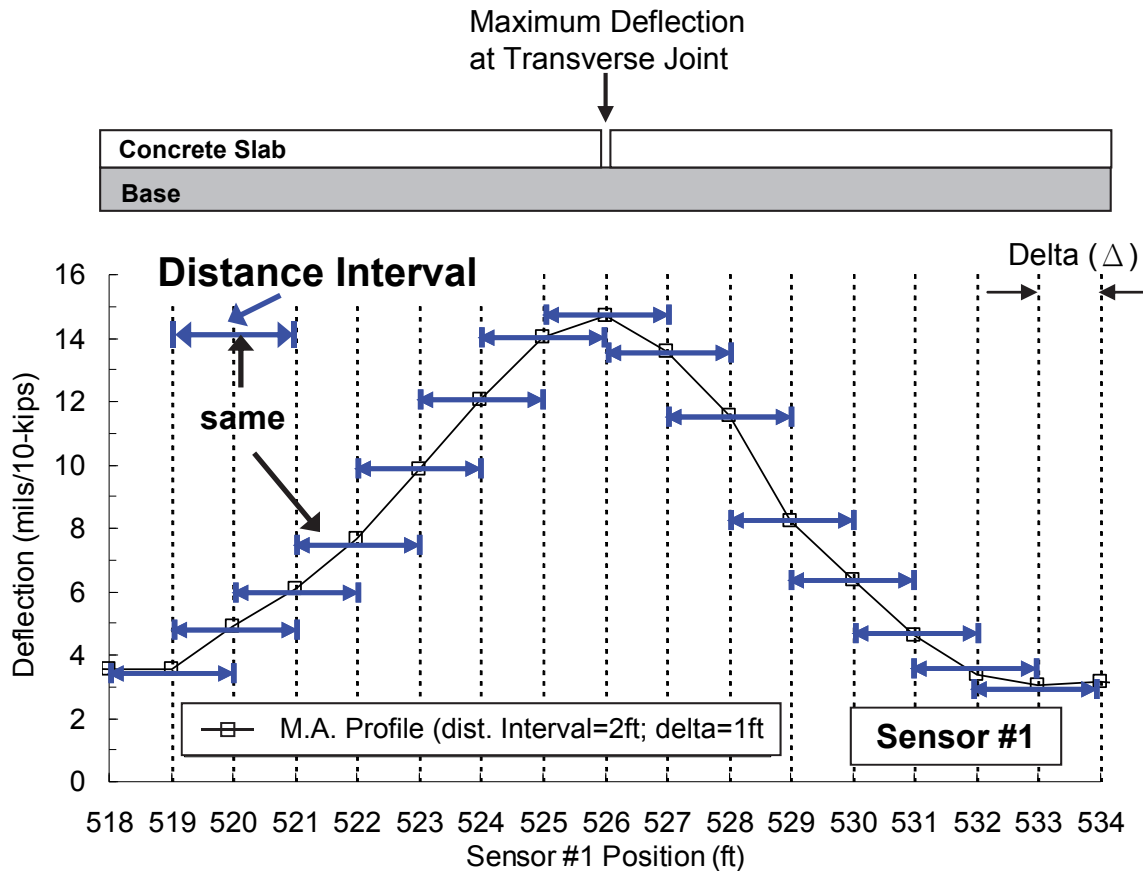
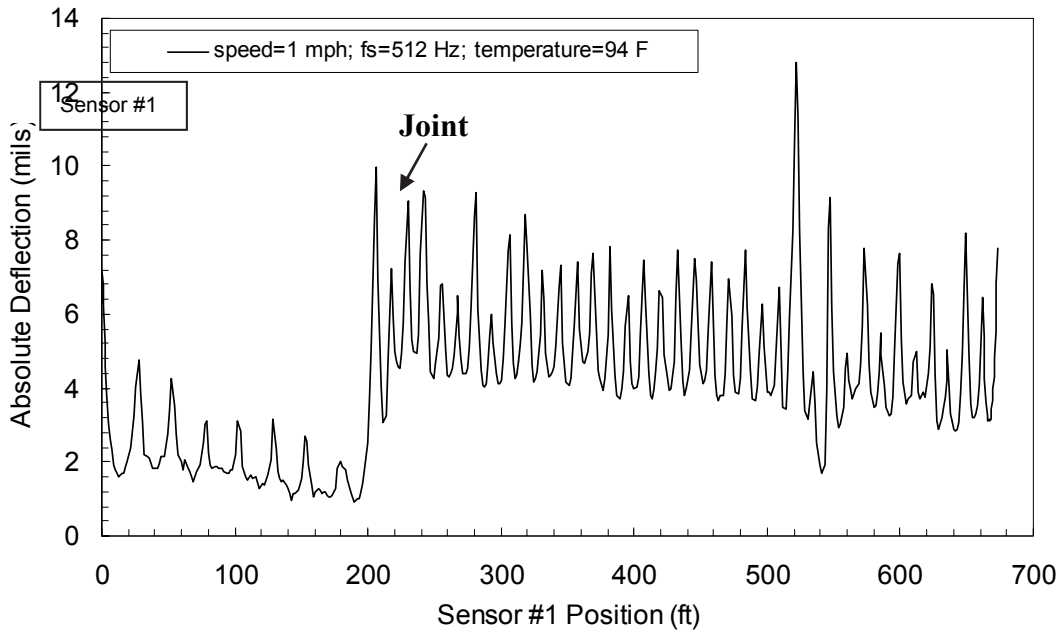


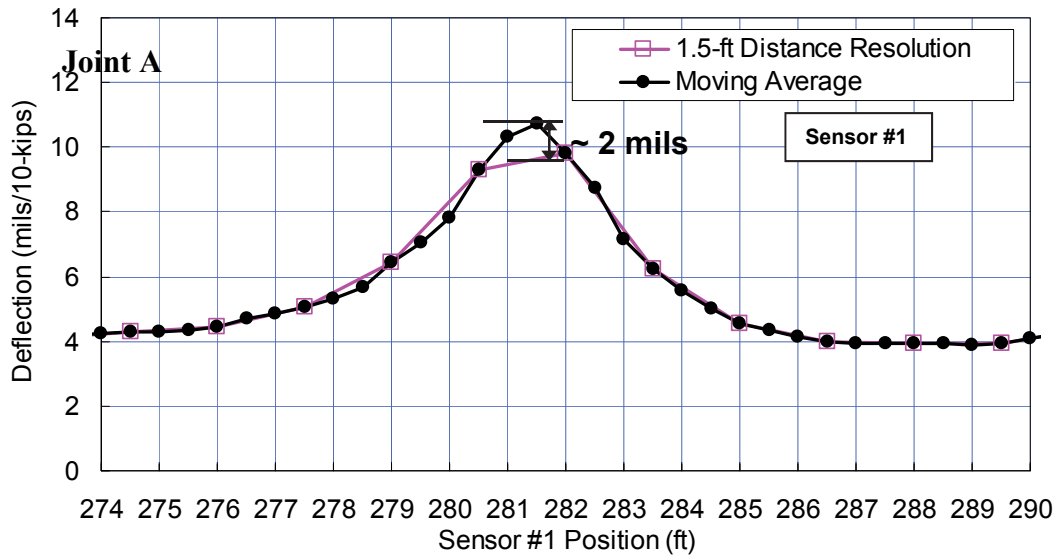
Figure 4.4: Expanded View of Moving Average Distance-Based Profile at a Joint; Distance Interval of 2 ft and Delta (Δ) of 1 ft

If one assumes a testing speed of 1 mph, then distance intervals of 1.5 and 3 ft approximately correspond to the time intervals of 1 and 2 seconds, respectively. A distance interval of 1.5 ft with a delta of 0.5 ft would be reasonable for a low testing speed of 1 mph. However, the rolling noise dramatically increases with increasing testing speed. Hence using the same distance interval of 1.5 ft may not be acceptable with respect to noise filtering. Increasing the distance interval results in narrower BW_{20} (more noise filtering) but this change results in a longer settling time of the notch-pass digital filter. Thus, an optimum combination of design parameters for the moving average analysis (distance interval and delta, Δ) is vital so as not to lose both spatial resolution and filter performance (noise attenuation).

Two case studies that involve different values of distance interval and delta were used to show the advantages of the moving average method. The raw data used in the two case studies were from continuous RDD profiling along a JCP using the new rolling sensor (Sensor #1) at the speeds of 1 and 3 mph, respectively. The distance interval of 1.5 ft and its delta (Δ) of 0.5 ft were used with the speed of 1 mph while a distance interval of 3 ft and a delta of 1 ft were used for a speed of 3 mph. The analysis results of Cases 1 and 2 are shown in Figures 4.5 and 4.6, respectively. In these figures, the time-based deflection profile and the moving average distance-based profile are compared. As shown in Figure 4.5b, the difference between the maximum and minimum deflections at Joint A is approximately 2 mils, which is about 18 % of the measured RDD deflection. This observation indicates that the old data analysis (time-based method) often results in an underestimation of deflections at joints/cracks. As the distance interval increases, the deflection difference at joints tends to decrease because of the “averaging effect” that involves more mid-slab areas. Based on the results, it can be concluded that the moving average profile identifies and measures the joint deflection in a more accurate manner. In addition, the moving average deflection profiles improve the spatial resolution without sacrificing the filtering performance, which is indispensable in attaining the higher testing speeds.

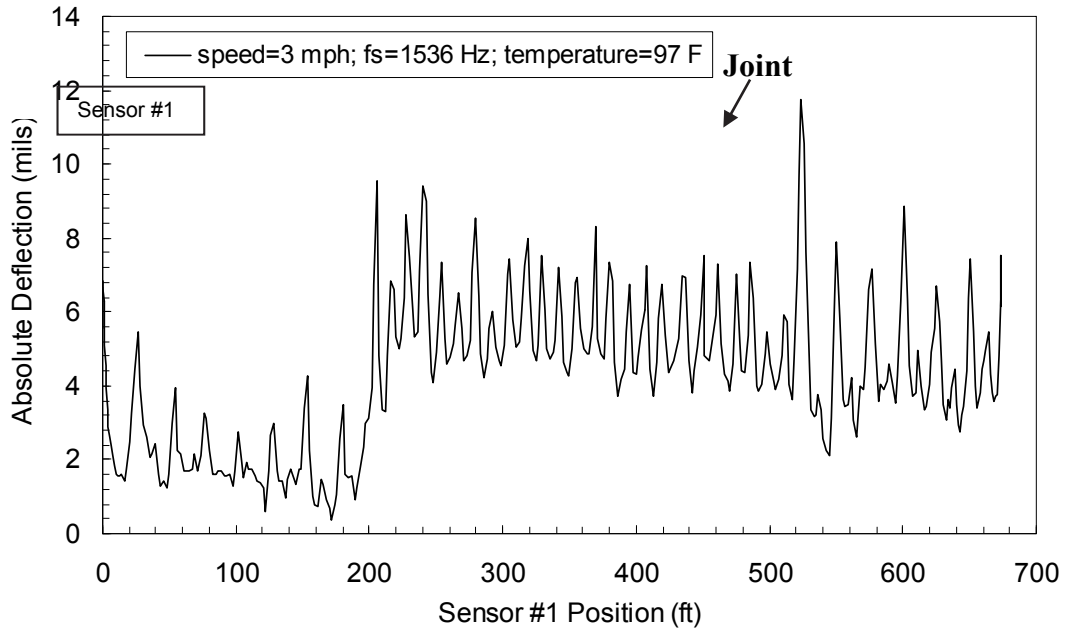


(a)

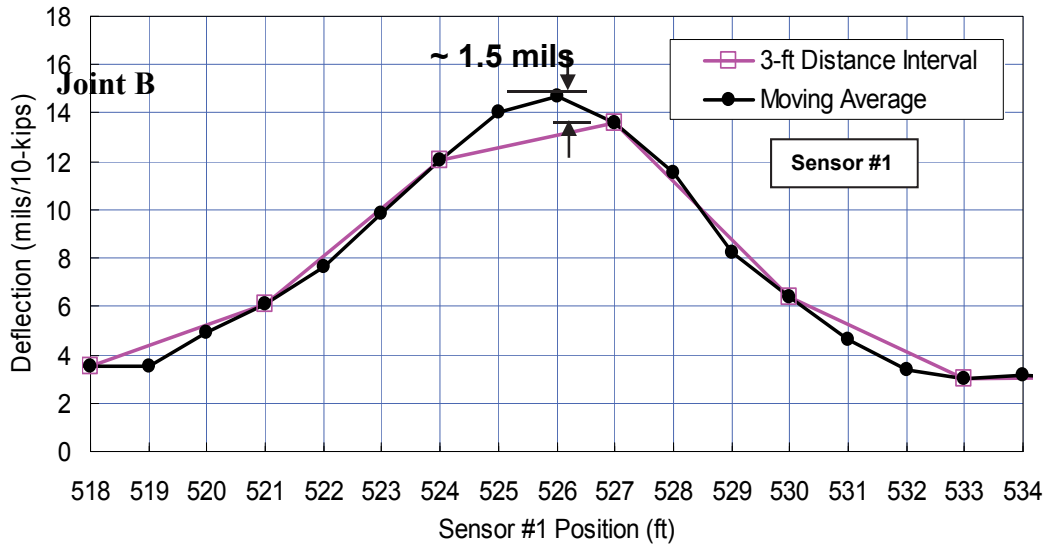


(b)

Figure 4.5: RDD Deflection Profiles at a Speed of 1 mph: (a) Moving-Average Deflection Profile (Distance Interval of 1.5 ft and Delta of 0.5 ft) along Path E and (b) Expanded View of Moving-Average and Time-Based Deflection Profiles at Joint A



(a)



(b)

Figure 4.6: RDD Deflection Profiles at a Speed of 3 mph: (a) Moving-Average Deflection Profile (Distance Interval of 3 ft and Delta of 1 ft) along Path E and (b) Expanded View of Moving-Average and Time-Based Deflection Profiles at Joint B

Chapter 5. RDD Data Acquisition Software Development

5.1 Introduction

In 2009, TTI researchers bought all of the components required for the TPAD data acquisition software development. These components were assembled into a working prototype system and a series of laboratory and field studies were conducted to determine if they were capable of handling the mass data collection needed for the TPAD's deflection sensors. Initially, a laboratory simulation system was developed to make sure that the proposed system has sufficient capabilities and stability prior to conducting field tests. As reported in last year's <Year 1> report these preliminary tests were successful. In FY 2010, the final components were assembled and a trial installation was made on the original TPAD unit. In addition, this work has continued during the TPAD construction. The software and hardware developments and test trials are described below.

5.2 Software Development

After the TTI team developed the first version of the TPAD software in 2009, continued testing of this software was done in 2010 to improve the software with the simulator device. Many bugs were fixed and the software was used to collect data for an extended period of time. Also, new functions were added to the preliminary version of the software. These new functions include:

- Addition of new TPAD data channel setup and configuration dialog box to the data acquisition software. The benefit of this is that the operator can control the channel name, reporting unit, chart maximum and minimum value of the TPAD data collection (see Figure 5.1).
- Changes to the DMI processing method for converting the digital pulse counts to the analog processing method. The new method can let two systems share the same DMI source. Also this change will increase the accuracy of the distance measurement (see Figure 5.2).
- Modify the software to automatically adjust the TPAD data format to only save the active channels. This modification will save a lot of disk space. The analysis software will use the TPAD channels configuration file to assist in correctly reading and processing the raw data file.
- Based on the field test data, a function was added to adjust the chart scales to present the data with suitable axes scales.
- The data acquisition screen shown while data is being collected is shown in Figure 5.3. The first version of the software fixed the camera video resolution to 640X480. However it was found necessary to change this based on the active screen resolution, this video size is now automatically adjusted to fit the screen.
- Modification of the software to allow it to run for extended periods, the initial version crashed when running over 40 minutes.

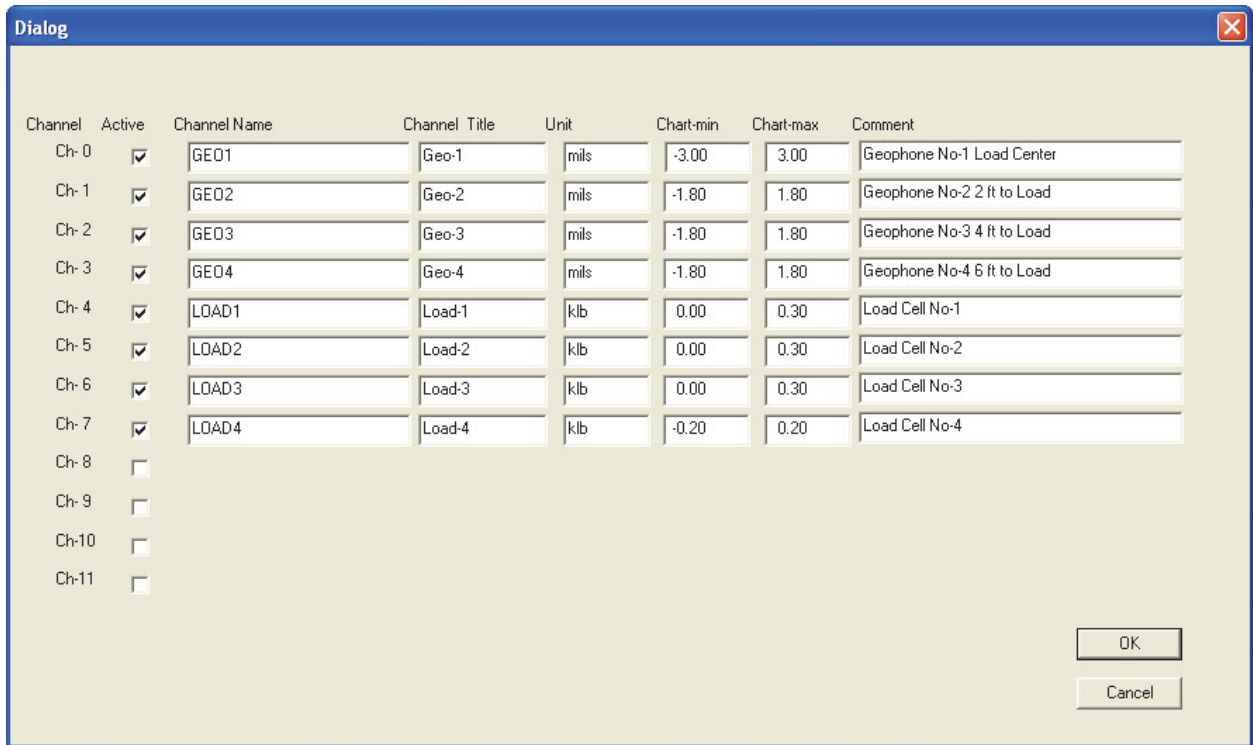


Figure 5.1: TPAD Data Channel Setup and Configuration Dialog Box

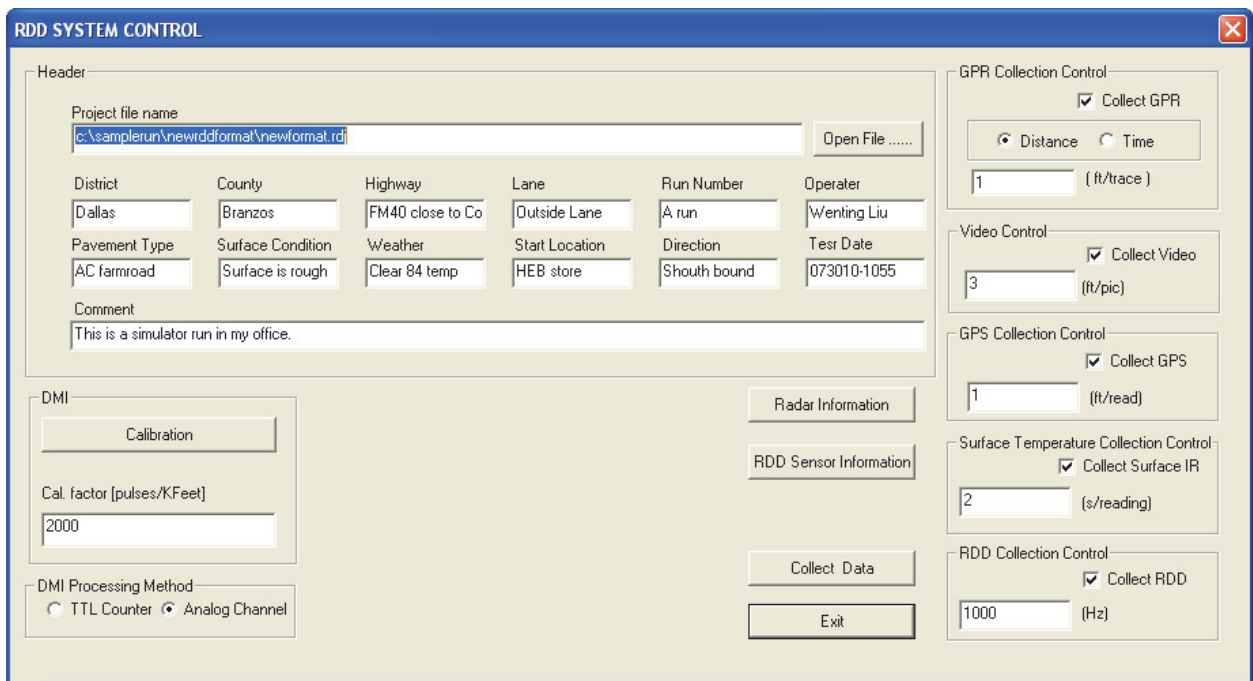


Figure 5.2: TPAD Data Acquisition Control Screen

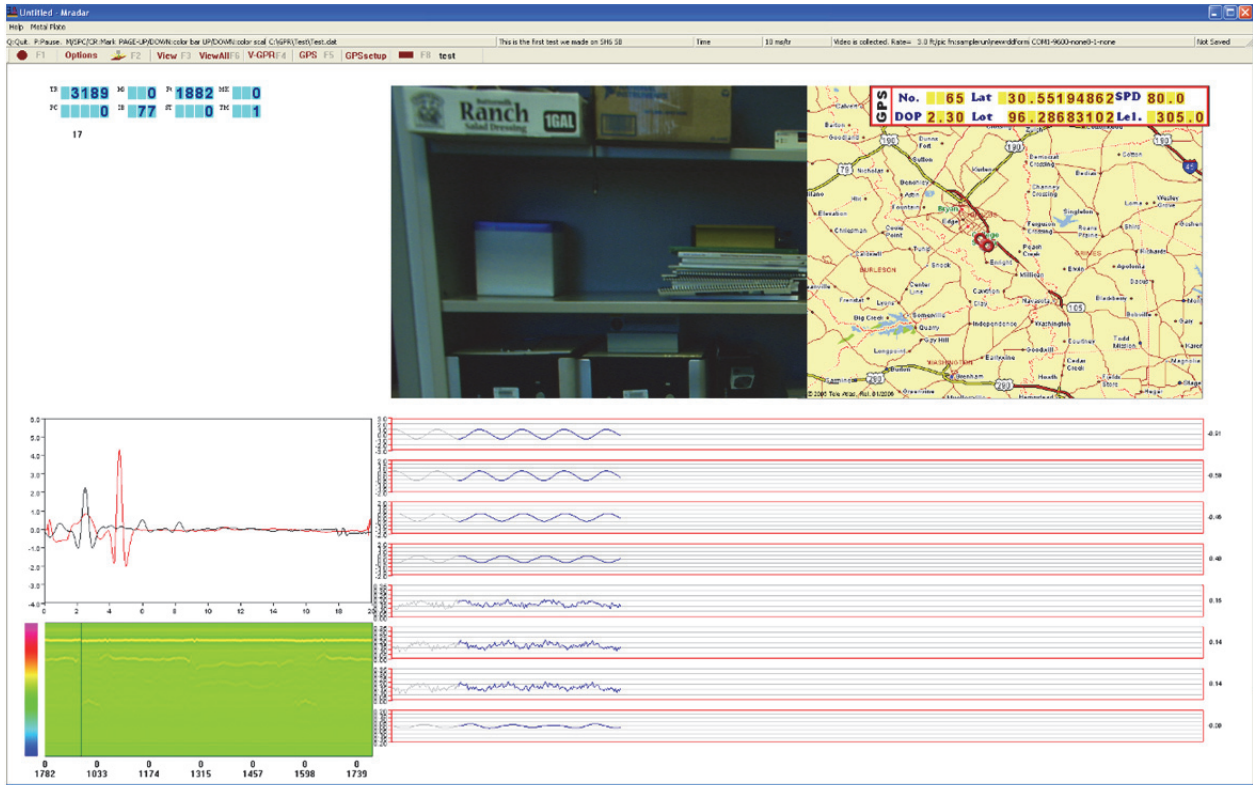


Figure 5.3: Real Time TPAD Data Acquisition Screen

5.3 Hardware Development

Based on the components that were purchased in the first year, the TPAD data acquisition hardware system was redesigned. The setup diagram is shown in Figure 5.4. To avoid excessive clutter, a control box to house all of these small components and cable connections was designed and constructed (see Figures 5.5 and 5.6).

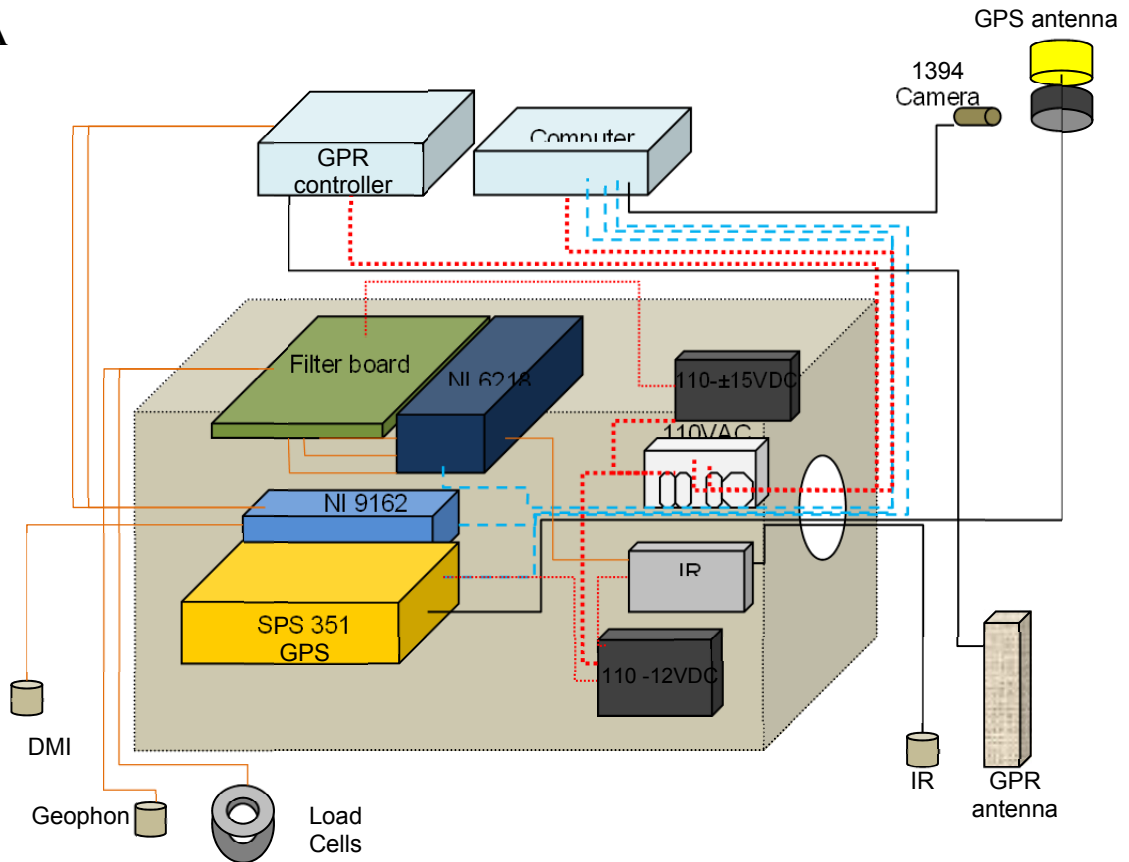


Figure 5.4: TPAD Data Acquisition Hardware System Setup Diagram

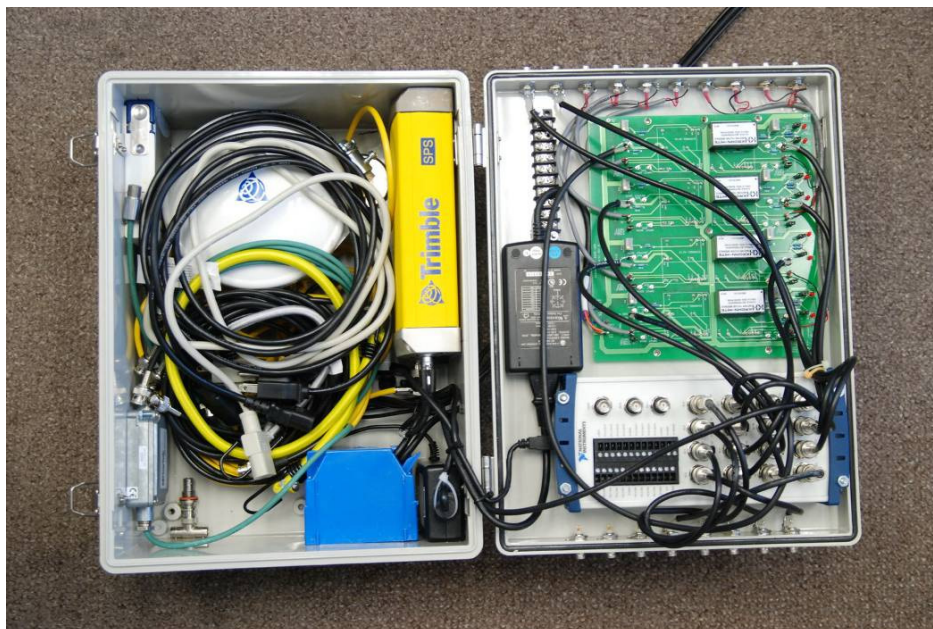




Figure 5.6: TPAD Data Acquisition Instrument Box (When Closed)

Also the GPR manufacture was contacted to re-design the GPR control box. Figure 5.7 is a photograph of the newly designed GPR control box. The size of the new box is less than one third the size of the old GPR control box. This change will save space inside the TPAD vehicle.



Figure 5.7: New GPR Control Box for the TPAD Data Acquisition System

In this prototype system the data acquisition computer to be installed in the TPAD will be an industrial grade panel mounted computer. The software/modifications to be installed on this computer are listed below.

- National Instrument Device driver system NI-DAQmx 9.0.
- Fire wire 1394 industrial camera driver from National Instrument.
- USA Tele Premium mapping data for the map display purposes.
- Change the XP system setting to increase the efficiency.
- Install the TPAD data acquisition software.
- Install a backup the hard drive for data security purposes.

This computer, with the loaded software, was given to Industrial Vehicles Inc (IVI) to mount in the new vehicle in late Fall, 2010.

5.4 Field Testing of New TPAD Data Acquisition System with the Original TPAD

In FY 2010, the data acquisition system developed by TTI was field tested with the original TPAD unit. As shown in Figure 5.8, a GPR antenna was mounted in front of the TPAD and a camera and GPS system were mounted on the roof. The data acquisition system was installed in the passenger seat of the TPAD. The first-generation geophone rolling sensor system was also installed under the unit as shown in Figure 5.9.



Figure 5.8: Mounting the GPS, GPR and Digital Video System on the Original TPAD Unit



Figure 5.9: Loading Roller and Rolling Sensors Arrangement Used in Testing

Testing was conducted at the TxDOT FSF facility near Austin’s main airport. The test path shown in Figure 5.10 was used to test the new data acquisition system. This test path had been used in previous studies and is known to consist of slabs with varying load-transfer efficiencies.



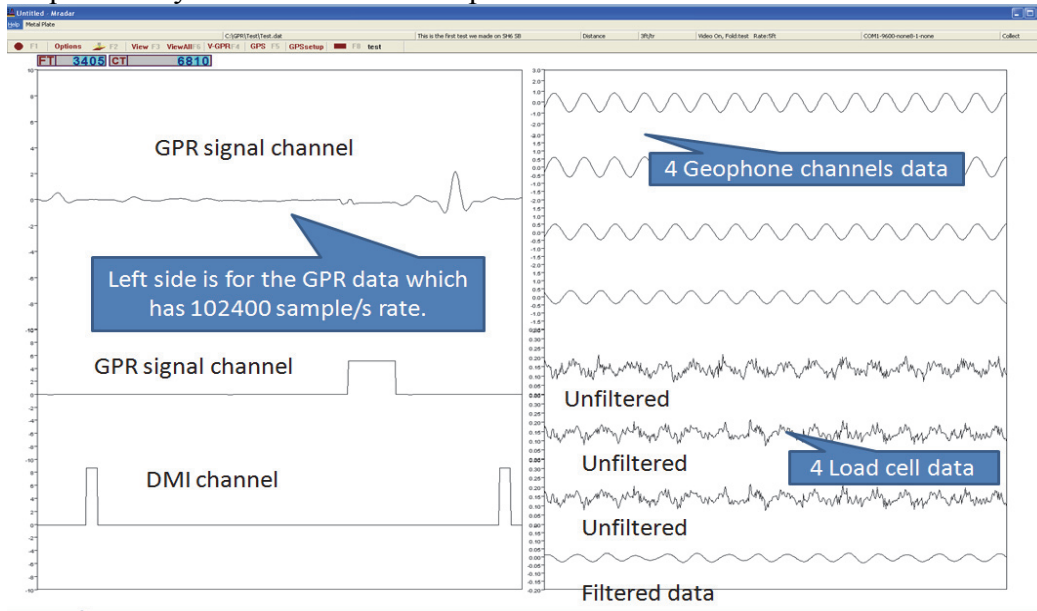
Figure 5.10: Test location and test path at TxDOT FSF

The data acquisition system described earlier was used to record the geophones on the rolling sensor as the TPAD passed over this section. In this test only one rolling sensor output was used and only two load cells were found to be operational. The data acquisition system has the capability of collecting four channels of load measurements and four rolling sensors outputs. In this test, repeat runs were made at three different speeds 1.0, 1.5 and 2 mph.

The raw data, shown in Figure 5.11, was collected and displayed during data acquisition. On the right of the figure, the four channels of rolling-sensor data are displayed. (These channels

are all the same as only on channel was collected in this run). At the bottom of the figure, the recorded raw load cell responses are displayed.

The raw data collected in each of the runs are displayed. The signals are similar in that the known problem joints had the biggest impact on the rolling-sensor output. However the data collected at 1 mph has significantly less noise than the data collected at 2 mph. No further analysis was conducted on this data since the purpose of the evaluation was just to ensure that the data acquisition system had sufficient capabilities to collect data in a field test.



Display of Raw data during data aquisition

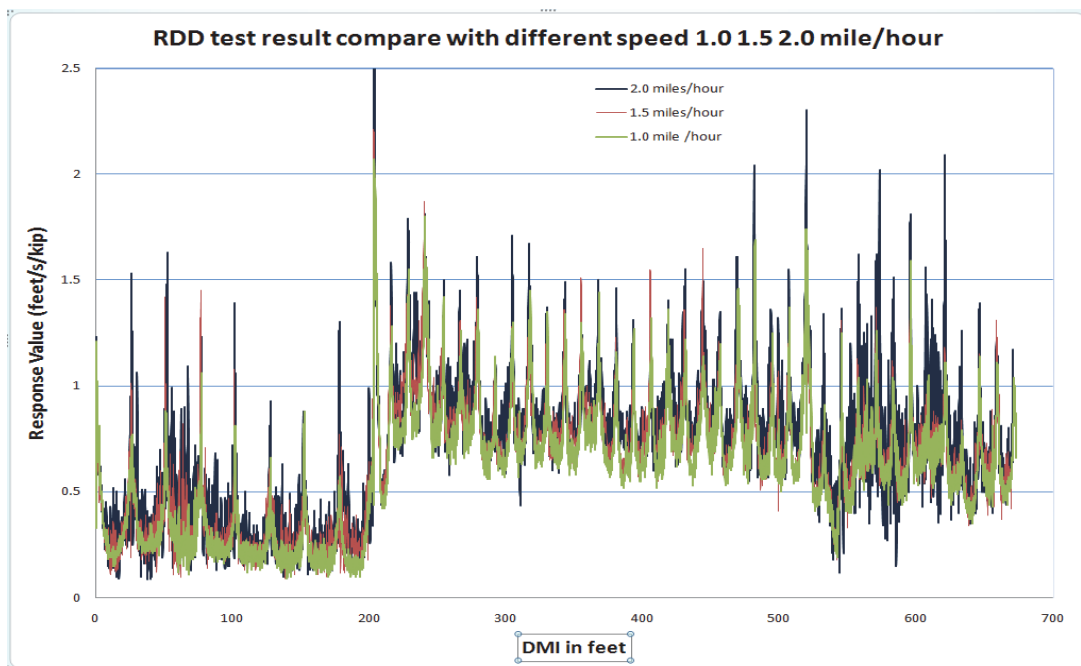


Figure 5.11: Geophone velocity data for each run

Chapter 6. Summary of Year 2 Activities

The activities during Year 2 have been successful and productive. The specifications, bid documents, bid acceptances, and purchase of the TPAD mobile platform and the TPAD transportation equipment (tractor and trailer) were completed by the CTR team. Construction of the TPAD is well underway and the acceptance testing will be done in early Year 3.

Various design parameters (hardness and thickness of urethane treads, and diameter and width of wheels) of the RDD rolling sensor have been designed and tested by the CTR and CEM team. In addition, improved bearings have been developed. The speed-improved rolling sensors have (1) a wider footprint, (2) rolling element bearings, (3) wider wheels for increase of contact area, (4) equal tread area on each side of the cart for better tracking, (5) more compliant urethane treads, (6) thicker treads, and (7) larger diameter wheels than the first-generation rolling sensors with 6 in. diameter wheels. Two combinations of wheel widths (4 in. and 2 in. versus 2 in. and 1 in.) and two options of wheel diameters (9 in. and 12 in.) have been constructed for flexibility in future testing. In addition, an active-actuator (voice coil actuator) concept was proposed by CEM for an improved rolling sensor hold-down system.

The performance of the newly designed rolling sensor was tested at various testing speeds at the TxDOT FSF and compared with the old rolling sensor in terms of measurements of rolling noise level. The newly designed sensor exhibited significantly lower rolling noise.

An improved data analysis procedure was also developed. The developed procedure involves the construction of deflection profiles that average over a distance interval and a distance interval is selected that moves continuously with the selected distance increment (distance-based analysis with moving average). Comparison of data processed with the old data analysis procedure (time-based analysis) with the moving-average, distance-based analysis shows that the new analysis procedure is superior, especially in identifying and measuring the joint deflections more accurately.

After successful simulator work, TTI made improvements to both the data acquisition hardware and software prior to field testing. On March 24–25, 2010, the TTI research team field tested the new TPAD data acquisition software on the original UT RDD. The field setup was successful and the collected data demonstrated the functionality of the system. Additional modifications were made to the data acquisition software based on the field testing and comments from CTR researchers. TTI researchers also updated the simulator's data with the new test data from the original RDD system.

On the hardware side in 2010, TTI researchers designed and built the control box to hold all components of the TPAD data acquisition system. Also, they worked with Wavebounce Inc. to design and build a new GPR controller that is much smaller than existing units. All of these components will be mounted onto the new TPAD system in Year 3.

References

Bay, J. A. (1997), "Development of a Rolling Dynamic Deflectometer for Continuous Deflection Testing of Pavements," Ph.D. Dissertation, The University of Texas at Austin.

Bay, J. A., and Stokoe, K. H. (1998), "Development of a Rolling Dynamic Deflectometer for Continuous Deflection Testing of Pavements," Publication FHWA/TX-99/1422-3F, FHWA/Texas Department of Transportation, Austin, Texas.

Chen, D.-H, Zhou, F., Lee, J. L., Hu, S., Stokoe, K. H., Yang, J. (2007), "Threshold Values for Reflective Cracking Based on Continuous Deflection Measurements," *Canadian Journal of Civil Engineering*, Vol. 34, pp. 1257-1266.

Lee, L. J. (2006), "Speed Improved Rolling Dynamic Deflectometer Testing and Analysis Procedures," Ph.D. Dissertation, University of Texas at Austin.

Nam, B. H. (2010), "Improvements of the Testing and Data Analysis Procedures for the Rolling Dynamic Deflectometer," Ph.D. Dissertation, University of Texas at Austin.

PSI Urethane Inc., Hardness Chart and Physical Properties of Polyurethane, 2009.

Appendix A: Specifications for RDD Vehicle Portion of the TPAD

Vehicle: Shall be four wheel drive hydrostatically driven with planetary type drive axles with locking differentials. Vehicle weight shall not exceed 20,000 pounds. Vehicle shall have a diesel engine and equipped with the following:

- a. Electric servo speed control with a range of 1 mph to 10 mph and capable of controlling within +/- 0.2mph.
- b. Halogen headlights, backup lights, clearance lights and LED lamps for stop, turn and tail lights.
- c. Strobe light mounted on top of cab and 4 additional mini strobe bars (2 amber and 2 white) mounted on rear of vehicle above stop lights.
- d. There shall be a 12VDC waterproof connector on a 30 amp breaker wired to the area of the back bumper to power a sign board if needed.
- e. Windshield wipers with intermittent operational capabilities on both driver and operators side of vehicle.
- f. Fire extinguishers, minimum 10 pounds, UL rating ABC. The fire extinguishers shall be installed in a suitable and readily accessible location; two outside (at right and left sides) and one location inside.
- g. Vehicle shall be painted with gloss white paint.
- h. Vehicle shall have step integrated into front bumper to access roof for mounting camera.
- i. Ladder which can be folded will be installed at vehicle front. Location of ladder shall not obstruct the central area of front bumper where the ground penetrating radar will be located

Tires: Vehicle shall have R4 14.9X24 8-ply Turf tread tires or equivalent.

Cab: Shall be a minimum 142 cubic feet or larger two man cab equipped with the following:

- a. Air conditioner, heater and defroster. Air conditioner shall maintain a cab temperature of 68°F to support electronics and operations for continuous measurements over 8 hours. No rooftop air conditioner.
- b. Adjustable suspension seats for driver and passenger with seat belts attached to seats.
- c. Legal tinted windows and sun visors on both driver and operator side of vehicle.
- d. Minimum 6.5"X15" mirrors on each door with 6" round convex mirrors attached to bottom of each mirror.
- e. Three eternal dome lights with separate switches, one mounted above and forward of the driver and one mounted above and forward of the data operator and one mounted in center of cab inline with both dome lights.
- f. There shall be a 2,000 watt pure sine wave inverter (power inverter with continuous rating) located outside the cab in an environmentally protected enclosure. It shall be wired with the appropriate cabling in a manner that will allow a replacement to be

installed quickly. There also shall be three 12VDC flat connectors on separate 20 amp breakers installed near the instrument deck. A matching duplicate inverter shall be furnished with the vehicle upon delivery.

- g. Drawing of space required in cab for the TTI data acquisition system is shown in Figure A6.

Instrumentation: Unit shall be equipped with, but not limited to, the following gauges, indicators, and alarms. Wherever gauges are specified, indicator lights are not acceptable. If an electronic monitoring system is furnished which monitors the following minimum operating conditions, it is acceptable. All instrumentation shall be easily visible to the operator and labeled in English or show a universally recognized symbol for each specific gauge, indicator, or alarm function. Units equipped with instrumentation gauges shall have non-glare lights for night-time visibility. These are for the engine and hydraulic system:

- a. Engine temperature gauge.
- b. Voltmeter gauge.
- c. Engine oil pressure gauge.
- d. Hydraulic oil temperature gauge
- e. Fuel quantity gauge.
- f. Audible alarm and warning light for the following:
 - a. High engine temperature
 - b. Low engine oil pressure
 - c. Low hydraulic oil level in reservoir

Engine: Shall be a diesel engine and have a minimum of 115 horsepower @ 2,500 rpm continuous rating with minimum 291 ft lbs torque @ 1400 rpm and equipped with the following:

- a. Lubrication system for operating on steep angles of inclination not to exceed 45°.
- b. Insulated side panels shall be mounted on engine compartment for sound abatement. Noise levels shall not exceed state and federal regulations. Ref. 29 CFR subpart G starting at 1910.95.
- c. Minimum 180 amp alternator will be installed on the engine.
- d. Fuel system shall have a Racor water separator filter.

Fuel Tank Capacity: Minimum 40 gallons.

Hydraulic System: Vehicle hydraulic system provides minimum 3000 psi pressure to the vehicle drive system and the shaker unit and must meet the following requirements:

- a. Shall support continuous operations over an 8 hour testing day on Texas highways under extreme conditions over ambient temperature ranges from 20°F to 110°F.
- b. Shall operate with Panolin Saturated Ester Synthetic 46 Biodegradable hydraulic oil.
- c. Hydraulic oil reservoir shall have a desiccant breather mounted on reservoir fill cap to reduce moisture intrusion into reservoir.
- d. Hydraulic oil shall not exceed 170°F at ambient temperature of 110°F.

- e. A 12 VDC hydraulic pump shall be plumbed into vehicle hydraulic system to raise the loading system off the pavement in case of a main hydraulic system failure.

Safety Plaques or Decals: Product safety plaques and decals shall be affixed at the operator's station and at any hazardous area on the vehicle. The safety plaques or decals shall describe the nature of the hazard, level of hazard seriousness, how to avoid the hazard, and the consequence of human interaction with the hazard.

Specifications for RDD Dynamic Loading Unit Portion of the TPAD

Dynamic Loading Unit: Provides dynamic sinusoidal force and meets the following minimal requirements:

- a. Dynamic sinusoidal loading of 2,000 to 20,000 pound peak to peak.
- b. Operating sinusoidal frequency range: 20-50Hz.
- c. Shall provide a chirp function that operates from 7 to 200 Hz as in geophysical prospecting.
- d. Shall output sinusoidal forces with less than 30 percent total harmonic distortion at frequencies of 20, 30, and 40 Hz driving a rigid calibration block.

Dynamic Force Measurement: Install accelerometers to monitor the level of dynamic force level:

- a. Install redundant accelerometers on the mass and on the roller base frame. Each redundant pair of accelerometers shall be able to be: used separately, compared, and/or used as an average.
- b. Dynamic forces measured with accelerometers will be calibrated using a customized, dynamic load cell on which the loading rollers are placed.
- c. Calibration measurements will only be done when the vehicle is stationary.

Static Hold-Down System: Applies a static force to the two loading rollers and shall meet the following minimum requirements.

- a. Static hold-down force shall be adjustable from 2,000 to 12,000 pounds (within 500 pounds).
- b. Apply the static load to the loading rollers through air springs (or equivalent) to ensure compliance and isolation so that the suspended resonance of the vehicle is less than 2.5 Hz.

Static Hold-Down System Operations: The Static Hold-Down System shall be operated from the cab of vehicle. Operator shall have the ability to:

- a. Raise and lower the loading rollers from the cab of the vehicle.
- b. Monitor the loading rollers by video from the cab of the vehicle.
- c. Adjust the static hold-down on the loading rollers from 2,000 to 12,000 pounds (within 500 pounds).
- d. Static hold-down force will be based on hydraulic pressure measurement and will be calibrated with load cells so that a calibration curve can be established and loads can be resolved within 300 pounds.

Loading Rollers: Delivers static and dynamic forces to the pavement. The loading rollers shall meet the following minimum requirements:

- a. There shall be two loading rollers, each shall have a diameter of 18 inches and a width of 14 inches and shall be made of a 92 durometer shore A polyurethane material.
- b. General location of loading rollers is illustrated in Figure A1.
- c. Dynamic loads applied by the loading rollers shall be determined by redundant accelerometers installed on the moving mass and roller base frame. Each redundant pair

of accelerometers shall be able to be: used separately, compared, and/or used as an average.

- d. The dynamic loads measured using the accelerometer-based system shall be evaluated using load cells. The evaluation shall consist of averaging the peak-to-peak dynamic force over 20-cycle intervals in the steady-state portion of a 5-second time window. A total of 20 partially overlapping 20-cycle intervals shall be used in evaluating the accuracy of the accelerometer-based load measurement system. The average plus one standard deviation must be within 3.5% of the load-cell based measurement. The resolution is required at peak-to-peak dynamic loads of 6000, 8000 and 10000 lbs at frequencies of 25, 30, and 35 Hz.

Location and Clear Space Required for Sensing Rollers: The locations of the rolling sensors, areas of required space claim, and locations for mounting points are illustrated in Figures A2 through A6. Additional space, as shown by the red hatched boxes, must be provided around rolling sensors to accommodate the retraction / steering mechanisms as well as provide overhead space for the rolling sensors and mechanism to retract into. Suggested chassis hard points for mounting the sensor retraction / steering mechanisms are shown by the blue hatch boxes. Figure A5 details mounting points on the lifting frame for a center mounted sensor.

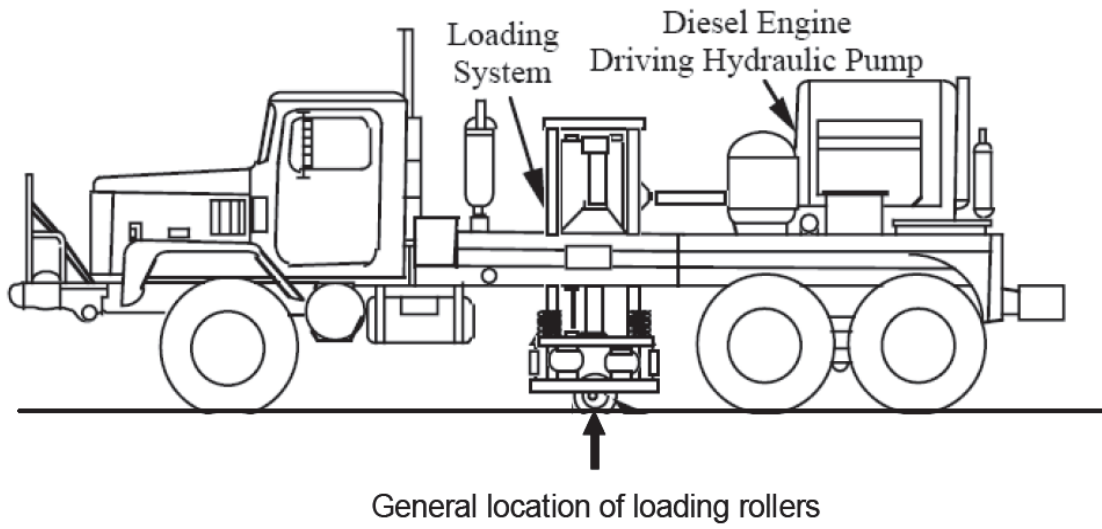
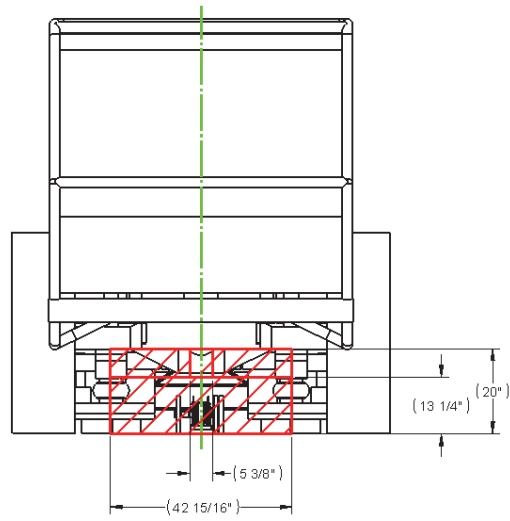


Figure A1: Location of Loading Rollers

Front View:



Side View:

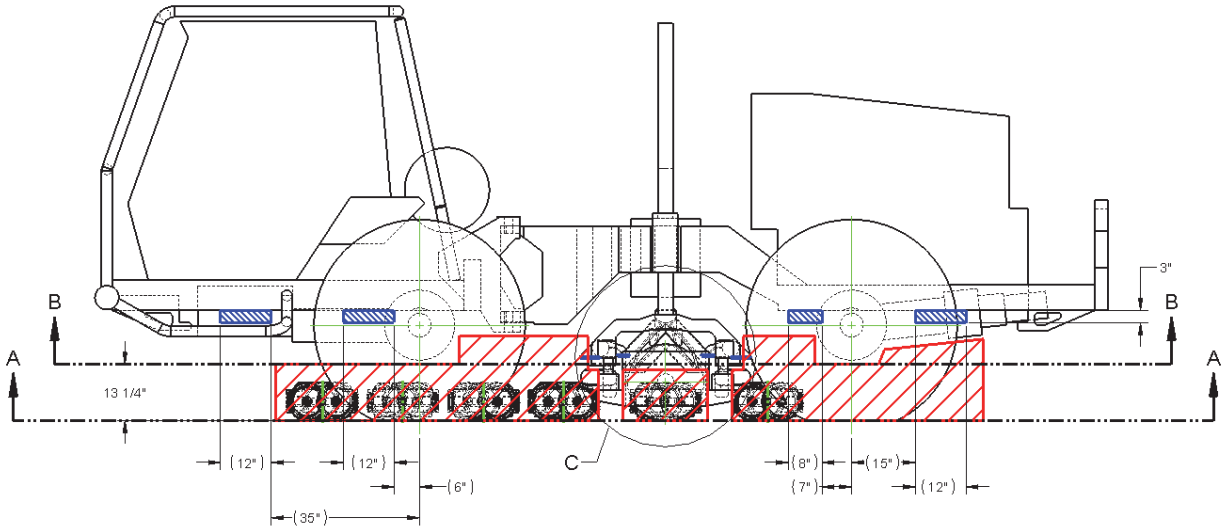
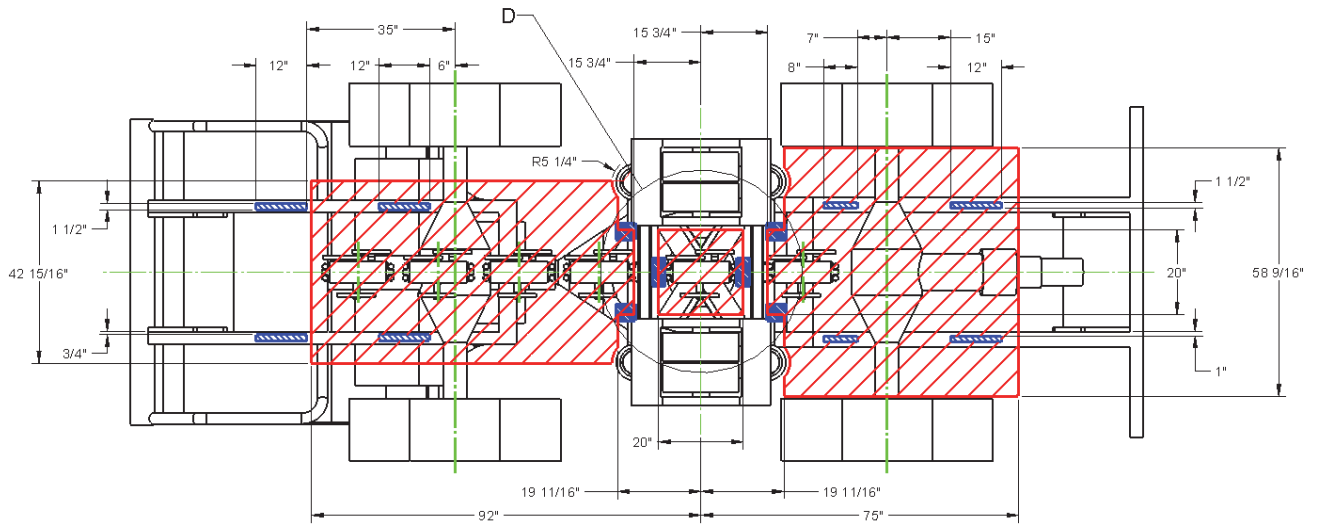


Figure A2: Front and Side Views

Bottom View at Section A-A:



Bottom View at Section B-B:

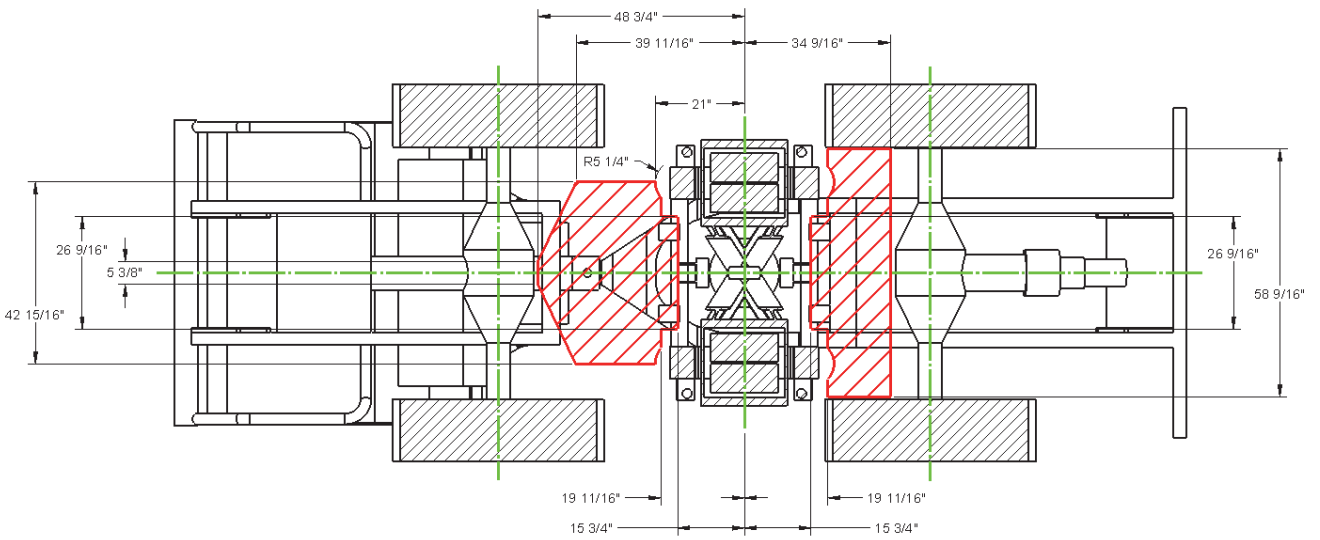
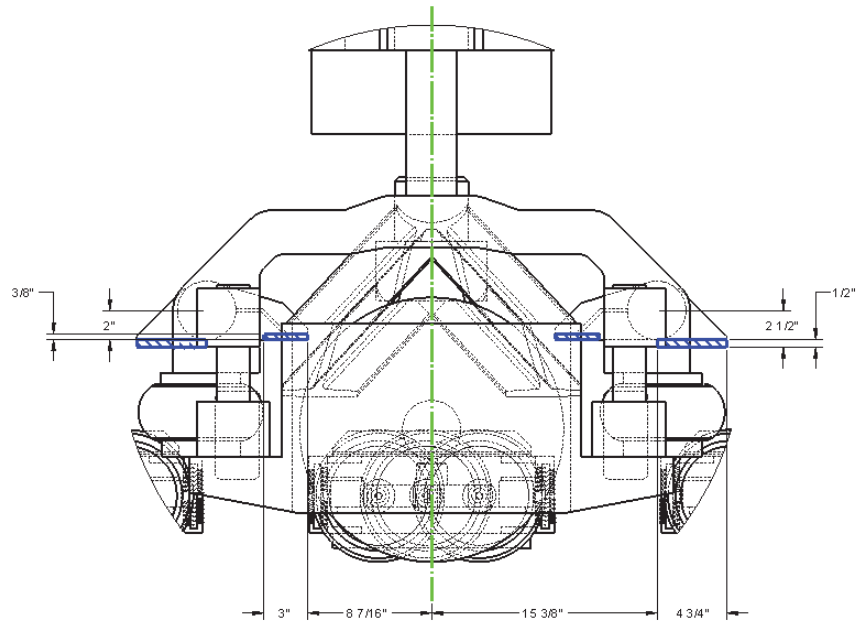


Figure A3: Bottom Views

Detail C from Side View:



Detail D from Bottom View at Section A-A

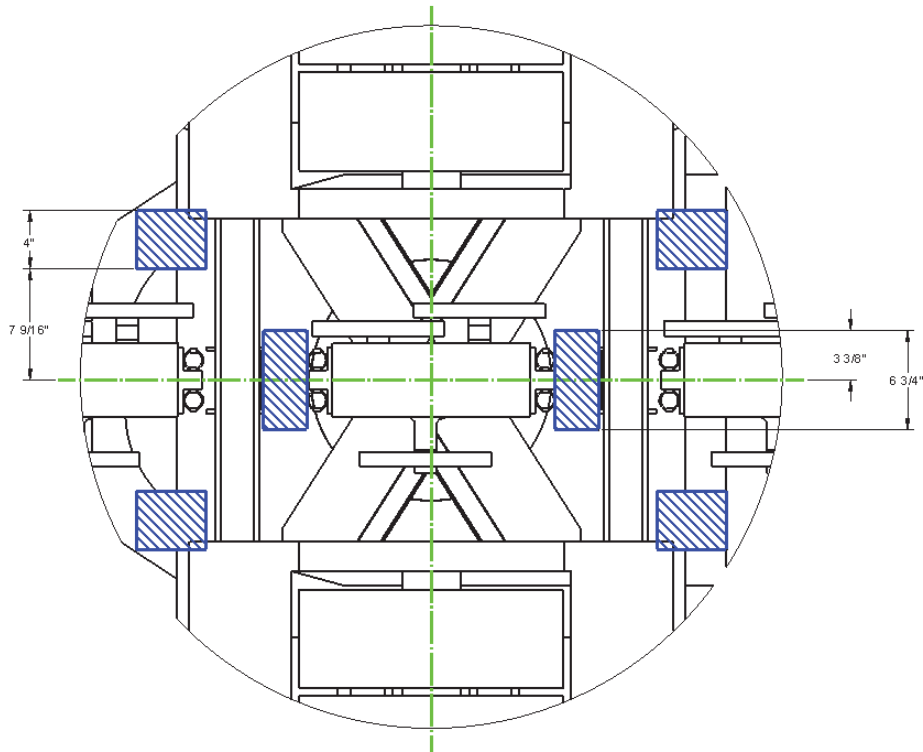


Figure A5: Detailed Views

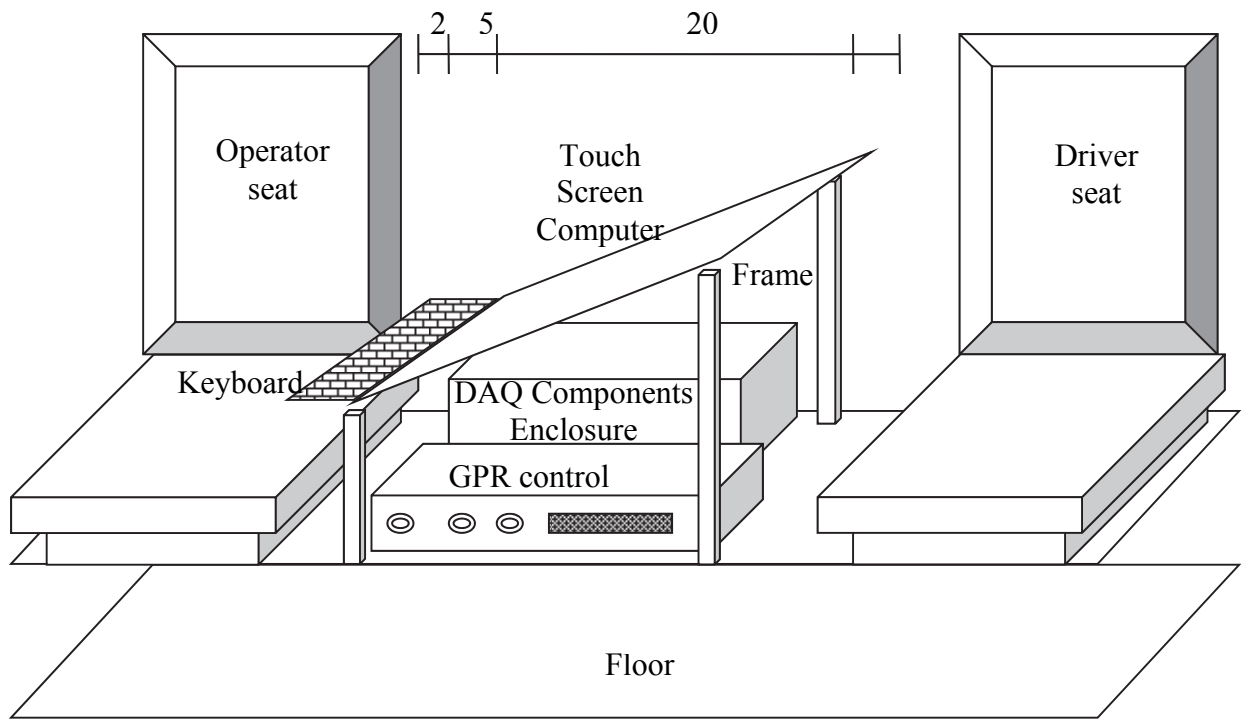
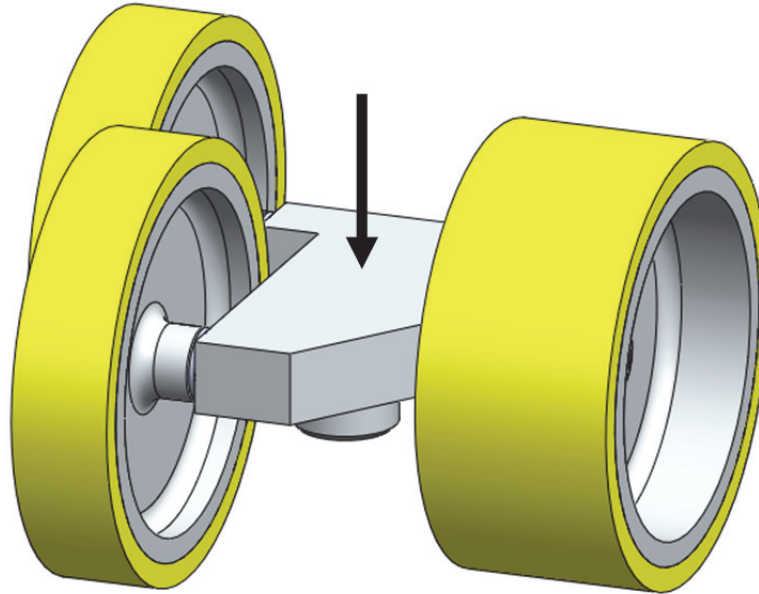
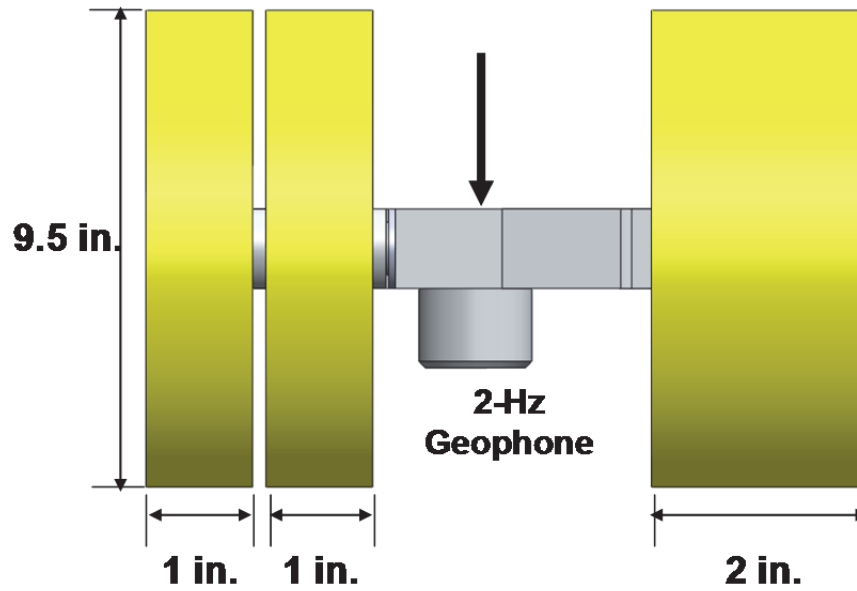


Figure A6: Space Requirement for TTI Data Acquisition System in Cab of New RDD

Appendix B: Design and Fabrication of Improved Rolling Sensor

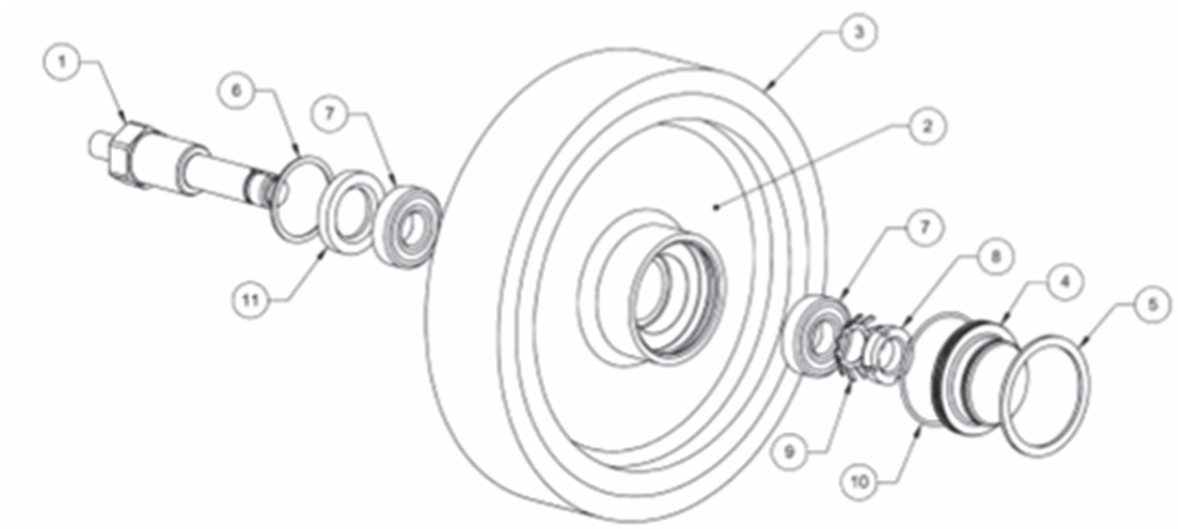


(a) CEM-Design Rolling Sensor

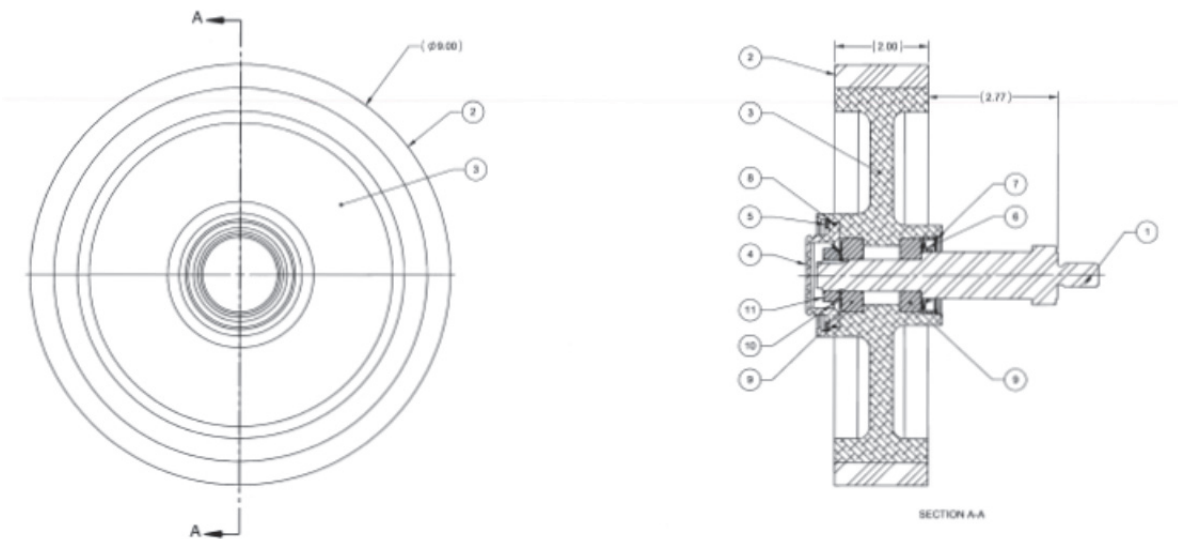


(b) Dimensions of the Sensor

Figure B1: New Rolling Sensor Designed by the CEM



(a) Sensor Wheel with New Bearing Set



(b) Cross-Sectional View of the Wheel and Bearing

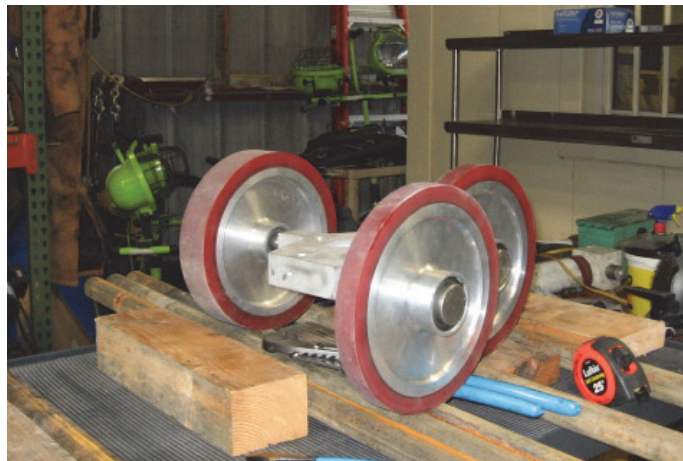
Figure B2: Mechanical Drawings of the Sensor Wheel and New Bearing Set



(a)



(b)



(c)

Figure B3: Photographs of the New Rolling Sensor of the TPAD